THE UNIVERSITY OF ALBERTA

RELEASE FORM

NAME OF AUTHOR JAMES LEWIS KENNEDY

TITLE OF THESIS IMPACT PRESSURES ON WEDGE SHAPED PROBES IN A RAREFIED GAS.

DEGREE FOR WHICH THESIS WAS PRESENTED M Sc.

YEAR THIS DEGREE GRANTED 1973

THE UNIVERSITY OF ALBERTA

IMPACT PRESSURES ON WEDGE SHAPED PROBES IN A RAREFIED GAS

by

JAMES LEWIS KENNEDY

A THESIS

SUBMITTED TO THE FACULTY OF GRADUATE STUDIES AND RESEARCH

IN PARTIAL FULFILMENT OF THE REQUIREMENTS FOR THE DEGREE

OF MASTER OF SCIENCE

DEPARTMENT OF MECHANICAL ENGINEERING

EDMONTON, ALBERTA

SPRING, 1973

THE UNIVERSITY OF ALBERTA

IMPACT PRESSURES ON WEDGE SHAPED PROBES IN A RAREFIED GAS

by

JAMES LEWIS KENNEDY

A THESIS

SUBMITTED TO THE FACULTY OF GRADUATE STUDIES AND RESEARCH

IN PARTIAL FULFILLMENT OF THE REQUIREMENTS FOR THE DEGREE

OF MASTER OF SCIENCE

DEPARTMENT OF MECHANICAL ENGINEERING

EDMONTON, ALBERTA

SPRING, 1973

THE UNIVERSITY OF ALBERTA

FACULTY OF GRADUATE STUDIES AND RESEARCH

The undersigned certify that they have read, and recommend to the Faculty of Graduate Studies and Research, for acceptance, a thesis entitled "Impact Pressures on Wedge Shaped Probes in a Rarefied Gas" submitted by James Lewis Kennedy in partial fulfilment of the requirements for the degree of Master of Science.

ABSTRACT

Experimental tests on wedge shaped impact probes were undertaken in a low density wind tunnel. The data obtained may be used to relate impact pressure readings to flow velocities in transition regime flows.

The wedge probes are of constant width and length with a rectangular orifice. The effect of varying the orifice height and the wedge angle were examined. The range of static pressure is from 30 to 300 microns and the Mach number range is from 0.1 to 0.4.

The viscous correction was found to decrease as the orifice height is increased. For a fixed wedge angle, the results could be correlated using the Reynolds number based on the equivalent diameter of the probe orifice. The results are compared with the experimental results of Pollard for circular cylinder probes. The viscous correction was found to decrease as the probe wedge angle is increased.

ACKNOWLEDGEMENTS

The author wishes to extend his appreciation to Dr. D.J. Marsden for providing the opportunity to undertake this project and for his guidance and supervision of this thesis. He also gratefully acknowledges the financial support of this research by the National Research Council.

Thanks are extended to the staff members of the Mechanical Engineering Shop, especially R. Beliveau and T. Simpson, and to Mary Sherban for typing this thesis.

Thanks are due to my wife, Marion, for her patience and understanding and for drafting the figures in this thesis.

TABLE OF CONTENTS

LIST OF FIGURES

LIST OF SYMBOLS

a	speed of sound
$\bar{c}$	average molecular speed
cm	most probable molecular speed
Cp	pressure coefficient for an impact probe
d	characteristics dimension
h	height of wedge probe orifice
H	height of water in manometer
Kn	Knudsen number
l	length of cylindrical probe
m	mass flow rate
M	Mach number
P_I	impact pressure on the probe
P_o	total pressure of the stream
P_s	static pressure
Q	volumetric flowrate through meter
r	radius of cylindrical probe
Re_d	Reynolds number based on probe diameter
Re_D	Reynolds number based on equivalent diameter
Re_h	Reynolds number based on orifice height
S	speed ratio
T	temperature
V	free stream velocity
α	probe wedge angle
γ	ratio of specific heats

λ	molecular mean free path
μ	viscosity
ρ	density

CHAPTER I

INTRODUCTION

The Pitot tube is used to measure the total pressure of a fluid stream assuming that the fluid is brought to rest isentropically at the stagnation point, which is at the face of the Pitot tube. This is, however, only true if the effects of viscosity can be neglected. The problem at low Reynolds numbers is that the viscosity can no longer be neglected and thus the stagnation pressure on the face of the Pitot tube can no longer be assumed to be the total pressure of the fluid stream. For an accurate measurement of the stream velocity a correction for these viscous effects will have to be applied to the Pitot tube readings.

There are three main areas of study in which viscous effects may significantly influence impact tube readings. The first area is where the size of the impact tube is very small, as in the measurement of velocities in boundary layers. The boundary layer is thin and the dimensions of the tube have to be small to make measurements within such a layer. The second is where velocity measurements are to be made in very viscous fluids such as lubricating oils or glycerine. The third is in low density gas flows with low Reynolds numbers.

The main body of experimental and theoretical work, from the first experimental investigation of Barker [1] to the recent results of Pollard [2], have been concerned with the use of cylindrical probes with circular cross sections. Some other shapes have been used, namely Homann's [3] use of spheres and circular cylinders placed transverse to the flow and MacMillan's [4] use of flattened cylindrical tubes. In a recent

work measuring boundary layer flows at low density, Berard [5] used a wedge shaped probe. His reasons for doing so were that in measuring the boundary layer on a flat plate he required a spatial resolution of 0.004 inches and the long response time of a circular cylinder probe of such a diameter in a rarefied gas would make such a probe impractical.

The practical possibilities of such a wedge probe due to its good spatial resolution and small response time make this type of probe excellent for use in two dimensional, rarefied gas flows. It is therefore highly desirable that the viscous correction to a wedge probe be determined.

The probe used here was symmetric rather than the asymmetric shape used by Berard because the asymmetric shape is difficult to build and it would probably have about the same characteristics as a symmetric probe. This change enables one to vary the orifice size, at the front of the probe, with ease. As probe geometry has been shown to be an important factor in determining impact pressures, provision was made to vary the wedge angle and the height of the orifice at the front of the probes.

The Reynolds number is important because the correction to impact pressure is an effect of viscosity. The Mach number will also be important because the flow speeds are in the compressible range. Although various gases could have been used in order to vary the viscosity this was not done. Reynolds number changes were brought about only by changing the density and velocity of the flow.

CHAPTER II

THEORY AND LITERATURE SURVEY

2.1 Classification of Flow Regimes

Fluid flow is classified by three non-dimensional parameters, the Reynolds number, the Mach number and the Knudsen number. The flows dependent on Reynolds number range from the inviscid flow at infinite Reynolds number to the inertialess or Stokes flow at vanishingly small Reynolds numbers. The Reynolds number is defined [6] as,

$$Re = \frac{\rho v d}{\mu}$$

when ρ is the density, μ the viscosity, V a representative velocity and d a characteristic dimension.

The Mach number is a measure of whether it is necessary to take into account the compressibility of the fluid and is defined [7] as,

$$M = \frac{V}{a}$$

where V is the velocity and a is the local speed of sound.

The Knudsen number classification of the flow of a compressible fluid indicates whether the gas acts like a continuous fluid or acts in a manner dependent on the molecular nature of the gas. The Knudsen number is defined [7] as,

$$Kn = \frac{\lambda}{d}$$

where λ is the mean free path of a molecule and d is a characteristic dimension.

The continuum regime is approximately defined as the regime where Kn is less than 0.1. The free molecular regime is defined as the regime where Kn is greater than the order of 1. The transition regime lies between the continuum and the free molecular regimes.

It can be shown from the kinetic theory of gases that the viscosity of a gas is given by,

$$\mu = 0.499\ \rho\ \bar{c}\ \lambda$$

where $\bar{c}$ is the mean molecular speed.

The mean molecular speed $\bar{c}$ and the sound speed a are related by,

$$a = \bar{c}\ \left(\frac{\pi\gamma}{8}\right)^{1/2}$$

where γ is the ratio of the specific heats of the gas.

Combining these two expressions yields the results that,

$$Kn = 1.26\sqrt{\gamma}\ \frac{M}{Re}$$

From the above equation it can be seen that as the flow approaches the free molecular regime the Knudsen number gets larger, corresponding to a lowering of the Reynolds number and hence to the increasing importance of the viscous forces compared to the inertia forces.

2.2 Review of Theory

From Euler's momentum equations for an inviscid fluid one can obtain Bernoulli's equation for a steady, incompressible flow,

$$P_o - P_s = 1/2\ \rho\ V^2$$

where P_o is the total pressure and P_s the static pressure.

Using the isentropic flow relations one can obtain Bernoulli's equation for a compressible, isentropic flow [7],

$$P_o = P_s\left(1 + \frac{\gamma-1}{2} M^2\right)^{\frac{\gamma}{\gamma-1}}$$

The impact pressure on a Pitot tube in such a flow is assumed to be equal to the total pressure, P_o. At low Reynolds numbers the viscous terms can no longer be neglected and the above equations are inadequate to describe the impact pressure measured by a Pitot tube.

No exact theoretical solutions for the effects of viscosity on impact tubes has been found so far. However, in the limiting case of low Reynolds numbers, Stokes neglected the inertia terms in the Navier-Stokes equations, and obtained the result that, for the case of incompressible flow over a sphere [6],

$$P_I - P_s = \frac{3}{2}\frac{\mu V}{r}$$

where P_I is the impact pressure, V is the free stream velocity and r is the sphere radius. This is more conveniently expressed in terms of a pressure coefficient Cp. Cp gives the amount by which the impact pressure at the stagnation point exceeds the total pressure of the free stream, hence

$$Cp = \frac{P_I - P_o}{1/2\ \rho\ V^2} = \frac{6}{Re_d} - 1$$

where Re_d is the Reynolds number based on the sphere diameter.

In 1936, Homann [3] studied the viscous flow around a cylinder and a sphere based on the application of the solution of the Navier-Stokes equations known as stagnation point flow. For the two dimensional case he found,

$$P_I - P_o = \mu\left(\frac{\partial v}{\partial y}\right)_\delta$$

where $\left(\frac{\partial v}{\partial y}\right)_\delta$ is the velocity gradient away from the stagnation streamline, $y = 0$, measured where this streamline enters the boundary layer around the body.

For the three dimensional, axisymmetric case he found that

$$P_I - P_o = 2\mu\left(\frac{\partial v}{\partial r}\right)_\delta$$

where $\left(\frac{\partial v}{\partial r}\right)_\delta$ is the radial velocity gradient measured where the stagnation streamline enters the boundary layer around the body.

The above two results were applied to the flow over a cylinder and a sphere respectively. On such blunt-nosed objects the boundary layer thickness at the stagnation point is small compared with the radius of curvature of the object and the boundary layer thickness can thus be determined using the boundary layer equations.

The results obtained are that, for a cylinder,

$$Cp = \frac{8}{Re_d + 0.647(Re_d)^{1/2}}$$

and for a sphere,

$$Cp = \frac{12}{Re_d + 0.643(Re_d)^{1/2}}$$

where Re_d is the Reynolds number based on the diameter of the object.

The next step in the analysis was made by Chambré [8] who made an allowance for the effect of compressibility. He found that for a sphere in a compressible fluid,

$$Cp = \frac{(12 - 2.109\ M^2)}{Re_d + 0.643(Re_d)^{1/2}}$$

while for a half spherical nose on a cylindrical tube he found that [9],

$$Cp = \frac{14.5 - 3.647\ M^2}{Re_d + 0.643(Re_d)^{1/2}}$$

As Chambré points out these results are not applicable to measuring fluid flow in a rarefied gas due to the fact that the fluid ceases to act like a continuum and the basic equations are no longer valid.

The problem of interpreting impact pressure readings in a free molecular flow has been tackled by Chambré and Schaaf [10] for the case of an open ended, flat faced, cylindrical impact tube. The assumptions made are that intermolecular collisions can be neglected both inside and outside the probe; the gas molecules striking the surface are diffusely reflected; there is no outgassing; the gas is in Maxwellian equilibrium, both outside the probe, while travelling with the macroscopic velocity of the stream, and inside the gauge volume where the pressure is measured; and a steady state has been attained.

The impact pressure read by a probe in a rarefied gas will depend on the mass flux into and out of the tube. Using a tube of length L and radius r, the mass flux per second of free stream molecules with a speed ratio S entering the probe is given [11] as,

$$m_1 = \frac{\rho_1\ Cm_1}{2\sqrt{\pi}}\ \pi\ r^2\ [\chi]$$

where $\chi = \exp(-S^2) + S\sqrt{\pi}\,(1+\mathrm{erf}(S))$,

and cm is the most probable molecular speed. Similarly the mass flux per second of gauge volume molecules, where S = 0, returning up the tube is given by,

$$m_2 = \frac{\rho_2\, cm_2}{2\sqrt{\pi}}$$

W(L/r,S) is defined as the probability that a molecule with speed ratio S will reach the opposite end of the tube of length L and radius r without returning to its source. Thus the mass flow from the free stream into the gauge volume is

$$m_1\, W(L/r,\, S)$$

and the mass flow escaping from the gauge volume to the free stream is

$$m_2\, W(L/r,\, 0)$$

When a steady state is reached these two mass flows will be equal, and using the ideal gas law and the relation

$$cm = \sqrt{2RT}$$

it can be seen that

$$\frac{P_2}{P_1} = \sqrt{\frac{T_2}{T_1}}\,\frac{W(L/r,S)}{W(L/r,0)} \cdot \chi \,.$$

The probability W(L/r,0) was first calculated by Clausing and values of this probability are given in [12]. The probability W(L/r,S) was calculated by Schaaf and Chambré [10] to be,

$$W(L/r,S) = bW(L/br,0) - \frac{S}{2}\left[\left(\frac{L}{br}\right)^2 + 2 - \frac{L}{br}\sqrt{4+\left(\frac{L}{br}\right)^2}\right]$$

where $b = 1 + S$.

The effect of the mass motion was taken into account by assuming that the free stream molecules strike the walls a further distance from the tube entrance than molecules with no mass motion. The ratio of these distances was taken to be (1+S):1.

In most cases the temperature of the gauge volume is the ambient temperature which, unless the gas is pre-heated, will be the gas stagnation temperature T_0. For adiabatic flow one can write,

$$\frac{T_0}{T_1} = 1 + \frac{\gamma-1}{\gamma} S^2$$

and the expression for the impact pressure becomes,

$$\frac{P_I}{P_s} = \left(1 + \frac{\gamma-1}{\gamma} S^2\right)^{1/2} \frac{W(L/r,S)}{W(L/r,0)} \chi$$

As Enkenhus has pointed out [11] this expression is greatly simplified when an orifice probe is used where $L \ll r$ and $W(L/r,S) = W(L/r,0) = 1$. In this case the expression becomes,

$$\frac{P_I}{P_s} = \left(1 + \frac{\gamma-1}{\gamma} S^2\right)^{1/2} \left[\exp(-S^2) + S\sqrt{\pi}\,(1+\mathrm{erf}(S))\right]$$

2.3 Review of Experimental Work

The first experimental investigation on the effects of viscosity on impact pressure readings was that of M. Barker [1] in a range of Reynolds numbers from 10 to 100, in water. She was able to show that

for Reynolds numbers less than 60, the pressure coefficient, Cp, became positive by an amount that was no longer negligible. Homann [3] performed some experiments on both cylinders and spheres in oil between Reynolds numbers of 5 and 200. The results showed excellent agreement with the theoretical equations which he developed.

The results of Hurd, Chesky and Shapiro [13] for an open ended, flat-faced, impact tube in various oils of different viscosities shows the expected effect of the pressure coefficient becoming positive for Reynolds numbers below 80. A hitherto unobserved result was noted that the pressure coefficient became negative between Reynolds numbers of 100 and 3000. This phenomenon cannot be explained by any of the theories so far presented.

Later MacMillan [4] tried to duplicate the results of Hurd et al. but was unable to detect a negative pressure coefficient although he traversed a Reynolds number range from 30 to 2000. Also the pressure coefficient which he obtained was considerably larger than that of Hurd at the same Reynolds number, based on the outside diameter of the probe. However when the results are plotted using the internal diameter as the characteristic dimension the two sets of results are in much better agreement. This led MacMillan to believe that the viscous effects depended more on the internal diameter than on the external one.

In a further set of experiments MacMillan [4] flattened the round probes making three probes with orifice width to height ratios of 3, 7 and 11. These probes were tested over a Reynolds number range of 5 to 800, the Reynolds number being based on the internal height of the orifice. Each probe gave negative pressure coefficients over part of the range of the test, with the pressure coefficient becoming positive

for the lowest Reynolds numbers tested. There was very good agreement between the probes with width to height ratio 7 and 11 which led MacMillan to believe that the results for these probes represented the limiting values for large width to height ratio.

The experimental work was extended into the compressible flow field by Chambré and Smith [9] who tested their formula for the case of a cylindrical impact tube with a hemispherical nose. Comparing the actual mass flow through the nozzle of their wind tunnel with that calculated from the impact pressure distribution across the face of the nozzle they achieved a satisfactory agreement and concluded that their formula was valid over the range tested.

In a series of tests on both source-shaped and flat-faced cylindrical impact probes Sherman [15] showed that the flat-faced tubes had a lower pressure coefficient than the source shaped tubes at the same Reynolds number, based on the outside diameter. This was true for both subsonic and supersonic flows over a Reynolds number range from 2 to 800. He also found good agreement between his results for source shaped probes and Homann's theoretical figures for spherical probes.

Enkenhus [11] made a series of tests on open ended impact probes with a 10° chamber on the front. From his subsonic tests he was able to show that none of the viscous theories agree with his results below a Reynolds number of 3, based on the outside diameter. Below this value the measured pressure coefficient is lower than that predicted by the theories. His results span the range of Reynolds numbers from 10 to 0.1 and even at this latter figure the pressure coefficient was far from reaching the values predicted by free molecular theory. However the

readings from orifice probes agreed well with the free molecular theory developed for them when the probes had Knudsen numbers greater than 6.

A recent set of results on subsonic probes by Pollard [2] covered a larger portion of the transition regime than had ever been possible before, the results tending to the theoretical limits at both the free molecular and continuum ends. The probes used were flat-faced circular cylinders with an internal to external diameter ratio of 0.55 and a tube length to internal diameter ratio of 25.

Pollard used thermal conductivity gauges to measure his pressures and calibrated these against a McLeod gauge. Having a large stagnation chamber he was able to measure the total pressure directly, and was able to demonstrate that there existed an isentropic expansion from the reservoir to the test section.

One important result obtained by Pollard was that, for his probes, the viscous effect could be correlated by the equation,

$$\frac{P_I}{P_o} = 1 + 1.4 \frac{M}{Re_d} \quad \text{for } Re_d \geq 3 \ .$$

In checking this result with the figures of Sherman for a flat-faced probe, it can be seen that Sherman's data obeys the above relationship to within 4 percent.

In the present investigation the total pressure cannot be measured directly and for this reason the flows must be calibrated against some other standard. The standard taken was a probe as used by Pollard with the empirical relation which he gives for it. This was chosen because of the simplicity of the formula and its agreement with other experimental

work. For other probe designs there is not sufficient data available to use them as a standard. Also the agreement, where it existed, between theory and experiment did not go to a low enough Reynolds number to be of use in this investigation.

CHAPTER III

APPARATUS

3.1 The Low Density Wind Tunnel

A schematic layout of the low density wind tunnel is given in Figure 1 and a photograph of the tunnel in Figure 2. The tunnel shell is 24 inches in diameter and 6 feet long, it is constructed from 1/8 inch stainless steel. The settling chamber is a 12 inch diameter stainless steel cylinder 17 inches long fitted with removable nozzles at the entrance section.

The system is pumped by two Edwards 18B4 Oil Vapour Booster pumps which together can pump 5000 litres per second, these are backed by two Edwards ES 3000 mechanical pumps each capable of pumping up to 3000 cubic feet per minute. These latter pumps are also used as roughing pumps for the system. Between the tunnel and the vapour pumps there are baffle plates with a 4 inch diameter hole in the centre and 12 inch butterfly valves which are used to control the pumping speed.

The gas being used is obtained from gas bottles and passed into a large storage tank at a few p.s.i. above atmospheric pressure, then through a valve to the flowmeters. The flowrate is controlled by a metering valve and the gas passes through a coil of 1/4 inch diameter copper tubing into a diffuser mounted inside the settling chamber.

Schematic drawings of the two nozzles used in the wind tunnel are shown in Figure 3. The larger, 5 inch, nozzle was designed by Berard [5] to give a flow Mach number of 0.5 at the nozzle exit section at a static pressure of 100 microns for the maximum obtainable flowrate.

This nozzle was formed out of brass and has a 12 inch diameter flange which permits it to be mounted on the end of the settling chamber.

The smaller 3 inch nozzle was designed to give the same Mach number range at about three times the static pressure obtainable in the larger nozzle. This nozzle was made of aluminum and fitted inside the larger nozzle.

Each nozzle has a static pressure tap located 1/4 inch from the nozzle exit section. In the larger nozzle the static tap is a hole 1/4 inch in diameter with a length of 1/4 inch O.D. and 1/8 inch I.D. stainless steel tubing inserted in it. The tube is cut off flush with the internal surface of the nozzle and soldered in place. The smaller nozzle fits inside the larger nozzle and the static pressure tap is 1/4 inch diameter hole with a length of 1/4 inch O.D. and 1/8 inch I.D. stainless steel tubing inserted in it and cut off flush with the inside of the nozzle. A seal is made between the two static taps by a rubber 'O' ring held between the two pieces of tubing, the tubing in the smaller nozzle being held firmly in place by a screw.

The static pressure line is run from the larger nozzle through the 1/4 inch O.D. tubing to a point outside the wind tunnel where it can be connected to the various pieces of instrumentation.

The photographs, Figure 4, show the arrangement of a probe in the wind tunnel. The probe support is mounted from a movable flat plate which allows for movement in the axial direction. The plate is propelled from outside the tunnel by an electric motor operating through a mechanical seal, with a series of gear reductions. The arm which supports the probe is mounted on a vertical slider, with a scale marked on it,

and on a long threaded rod. The probe can thus be traversed across the face of the nozzle by rotating the threaded rod through a rotary feed operated from outside the tunnel.

Each probe is mounted on a 5 inch long sting made from 1/2 inch diameter tube. The impact pressure line consists of this sting, a length of 1/2 inch diameter tube, a 12 inch length of 1/2 inch diameter flexible tubing and a length of 1/4 inch diameter tubing running through the tunnel wall. The intermediate length of 1/2 inch tubing is connected by rotatable seals to the sting and the flexible tubing. The seal at the flexible tubing end is constrained to move horizontally, this allows the probe to be moved vertically over large distances while the flexible tubing is moved only fractions of an inch. By having a small motion of the flexible tubing the stresses on the probe support arm are small and the probe alignment does not change as one traverses the nozzles.

3.2 The Probes

A drawing of the static pressure probe is given in Figure 5, this probe design is based on the recommendations made by Merriam and Spaulding [16] and used by Sherman [15]. Also in Figure 5 is a drawing of the impact pressure calibration probe. This is an open ended, flat-faced, cylindrical tube with an internal to external diameter ratio of approximately 0.55 and a probe length to internal diameter ratio of 25 when mounted on the sting. The viscous correction to such a probe has been studied by Pollard [2] and his results were used in the calibration of the flows in the wind tunnel.

An exploded view of a wedge probe is given in Figure 6, this particular model has a wedge angle of 8°. The probes were symmetric wedges,

5 inches long and 5/8 inches wide, with wedge angles 8°, 16°, 24°, and 32°.

The wedge bodies were cut from stainless steel plate and machined to the correct angle with a tolerance of 0.01°. The wedge was then machined to 5/8 inch and a 3/8 inch slot cut in it to a depth of 4 inches from the apex. A hole was drilled and tapped, 1/8 pipe tap, in the base for connection to the probe support and impact pressure line. A 'Vee' groove, 0.03 inches deep was cut in both top and bottom faces around the 3/8 inch slot in order to retain the epoxy glue.

The top and bottom faces of the probe were manufactured from 0.020 inch stainless steel shimstock cut in 5/8 inch strips. One end of each strip was then ground to an angle of 4°, 8°, 12°, 16° for the four respective wedge angles. The grinding was performed in a jig with the strip being sandwiched between two similar pieces of material. The grinding was continued until the sharpened edge was less than 0.001 inch thick and with less than 0.001 inch deviation from a straight edge when viewed under a microscope.

The two shimstock surfaces were joined to the wedge body by 'Torr-Seal' low vapour pressure epoxy resin which was placed in a continuous bead in the groove in the body. The glueing process was carried out in a jig which allowed the orifice height to be set at the desired value with feeler gauges. Any excess glue was removed from the probe. Figure 7 shows some of the completed wedge probes along with the static pressure probes.

3.3 Instrumentation

A 'C.V.C.' McLeod gauge, a temperature compensated N.R.C. 801

thermocouple gauge and one side of an M.K.S. Baratron capacitance manometer were connected to the static pressure line as can be seen in Figures 1 and 2.

The McLeod gauge was connected to the static pressure line by a length of 1/4 inch O.D. stainless steel tubing and was liquid nitrogen trapped. This gauge was used as the absolute standard to calibrate the thermocouple gauge. The thermocouple gauge head is mounted on the static pressure line through a short length of 1/2 inch O.D. tubing. A digital voltmeter with a resolution of 0.01 millivolts was used to measure the output of the thermocouple gauge.

The capacitance manometer head was mounted with one port connected to the static pressure line and one port connected to the impact pressure line. The differential pressure was measured using the pressure readout dials, which are a series of 3 decade switches and a potentiometer used to null the meter. By using a digital voltmeter the nulling process can be controlled accurately and a resolution of 0.05 microns can be obtained.

Two orifice meters were constructed to measure the gas flowrate into the wind tunnel. The larger meter has a 1/8 inch diameter orifice in a 6 inch long, 1/4 inch I.D. tube with the orifice 4" downstream from the tube entrance. The smaller tube has a 1/16 inch diameter orifice in a 3 inch long, 1/8 inch I.D. tube with the orifice 2" downstream from the tube entrance. The pressure drop across these meters was measured with a Betz manometer with a resolution of 0.05 mm of fluid. The two meters covered the range of gas flowrate required.

A Fischer Scientific Flowmeter kit was used to calibrate the orifice meters. The kit uses a series of rotameters and can measure flowrates over the range from 0.4 cc to 20 litres per minute.

The stagnation temperature was measured by a thermocouple mounted on the diffuser in the settling chamber. The thermocouple was made from 0.022 inch Iron-Constantan wire and the thermocouple E.M.F. read on a millivolt potentiometer.

CHAPTER IV

PROCEDURE

4.1 Static Pressure Gauge Calibration

In the experiments required to determine the viscous correction to the wedge probes it is necessary to be able to set the static pressure in the nozzle at particular values. A McLeod gauge is therefore not suitable for the task of measuring the static pressure because of the time required to take readings. Hence a temperature compensated thermocouple gauge was connected to the static pressure line.

The thermocouple gauge was calibrated against the McLeod gauge. For this the system was set up as in Figure 1 with both gauges connected to the static pressure line. The tunnel was pumped out with the booster pumps and the system flushed several times with the test gas. With the system pumped to its ultimate vacuum the McLeod gauge was outgassed using a soft flame. The butterfly valves were then closed and a small amount of test gas leaked into the system and the pressure allowed to stabilize. The stabilization took a few minutes and the capacitance manometer, with one side on the static pressure line and the other side connected to the inside of the tunnel, gave a good indication that the line and tunnel pressures had equalized.

The thermocouple E.M.F. and the McLeod gauge readings were noted and more gas was introduced into the system and the process repeated. Thus a calibration was obtained over the range of pressures from 15 to 350 microns. The calibration curve is given in Figure 8. The calibration was performed in a temperature range from 78°F to 82°F and, considering the magnitude of the pressures and the thermal compensation on

the gauge, the temperature should not affect the readings from the gauge to any noticeable extent.

4.2 Orifice Meter Calibrations

Due to the small size of the orifice meters used, the usual standards could not be applied in order to find the relationship between the pressure head across the orifice plate and the flowrate through the nozzle. It was therefore required to perform an experimental calibration relative to a previously calibrated rotameter.

The rotameter was inserted in the gas inlet line with its outlet connected, via a length of tubing, to the orifice meter inlet. A manometer was connected to the intervening length of tubing so that the pressure in the rotameter and orifice meter could be monitored.

The system was pumped out with the roughing pumps and gas leaked into the system through the metering valve. The pressure in the inlet line could be adjusted using a leak valve situated on the storage tank outlet, the pressure being monitored on the manometer. It was thus possible to keep the pressure in the line at 700 mm of mercury to within 0.2 percent. The temperature was kept between 78° and 82° for the duration of the calibration.

For several settings of the metering valve, readings of the orifice meter pressure head and the rotameter flowrate at 700 mm of mercury and 80°F were noted. Calibration curves of the pressure head and (pressure head)$^{1/2}$ versus the flowrate were drawn. This calibration was carried out for both orifice meters, and the calibration curves are given in Figures 9 and 10.

4.3 The Nozzle Calibrations

A static pressure profile across the face of the nozzle was measured with the static pressure probe to find the relationship between the stream static pressure and that measured at the wall tap. The system was first pumped out with the booster pumps until the pressure registered by the McLeod gauge was below 0.1 microns. The capacitance manometer was then zeroed. At this low pressure it was necessary to wait for a period of about 5 minutes for the manometer reading to stop drifting.

With the meter zeroed gas was allowed into the system through the metering valve. A series of tests at various flowrates and with various pumping speeds were carried out which covered the range required in the wedge probe calibrations. These tests showed that the static pressure at the wall tap was never more than 0.2 microns different from that measured by the static pressure probe in the centre of the nozzle.

No axial pressure gradient was detected between 1/4 inch upstream and 1/4 inch downstream of the static pressure tap. In a traverse across the face of the nozzle, the static pressure remained constant up to within 1/2 inch of the nozzle wall where the probe began to read pressures lower than that at the static tap. This result could be expected due to the blockage effect of the probe as it approaches the nozzle wall.

As the wedge probe calibrations were to take place in the centre of the nozzles at a position opposite the wall tap it was assumed that the pressure in the static pressure line gave the static pressure in the test area. The maximum error in static pressure reading was 0.2 microns, however the thermocouple gauge has a resolution of 0.3 microns and such changes would not show up on the static pressure gauge.

As the Reynolds number in the nozzle decreases, the boundary layer on the nozzle wall will thicken. There will be a certain Reynolds number below which the boundary layer will fill the whole nozzle and the velocity over the cross section is distributed in the form of a paraboloid of revolution. A central core of uniform flow at least as large as the probe width is required for these tests.

The cylindrical calibration probe was traversed across the face of the nozzle at several conditions of static pressure and flowrate, covering the test range, to determine the size of the useful core.

At large flowrates the boundary layer was thin and typically a central uniform core of 3 inches diameter in the large nozzle and 1-1/2 inches diameter in the small nozzle were achieved. In the worst cases the uniform core in the large nozzle extended over a 0.1 inch radius with pressure drop of 0.2 microns at a radius of 0.3 inches. In the small nozzle no uniform core existed but the pressure drop was 0.2 microns at a radius of 0.1 inches and 0.55 microns at a radius of 0.3 inches. As the internal diameter of the calibration probe is 0.274 inches and the orifice width of the wedge probe is 0.375 inches it was assumed that these probes would be in an essentially uniform core when on the nozzle centreline.

Three parameters are required to describe the flow in the nozzle: the temperature, the static pressure and the Mach number. The total temperature was measured at the diffuser on the gas inlet line. This remains at the ambient temperature which was kept between 78°F and 82°F.

With a particular flowrate through a nozzle, at a given static pressure there is a fixed Mach number on the nozzle centreline. The

nozzle calibration is performed to determine the relationship between this Mach number and the flowrate for a given set of static pressures.

The impact pressure calibration probe was set up on the nozzle centreline with its face lined up with the static pressure tap and connected to the impact pressure line. The system was pumped out with the booster pumps until the static pressure was of the order of 0.1 microns and the capacitance manometer was zeroed. With a known flowrate set up by the metering valve and read on the orifice meter, the pressure in the nozzle could be set at some desired level by operating the butterfly valves to the pumps. At each desired static pressure the system was given several minutes to stabilize. The nozzle static pressure and the impact pressure as measured by the capacitance manometer were noted. This process was repeated for several flowrates and for both nozzles. The results were then transformed, using the viscous correction formula given by Pollard [2], into a corresponding Mach number at the static pressure involved.

The results of this calibration are presented in Figures 11 and 12, these give the centreline Mach number at various nozzle static pressures as a function of the volumetric flowrate through the nozzle. Figure 11 refers to the large nozzle and Figure 12 to the small nozzle.

4.4 Test Procedure

Each probe was in turn mounted on the supporting sting with the probe orifice at a point, in the centre of the nozzle, opposite the static pressure tap. The tunnel was pumped out to better than 0.1 microns and the capacitance manometer was zeroed. The required condition of static

pressure and Mach number was then set up and readings of the static pressure and impact pressure noted. The static pressure was checked several times by the McLeod gauge and in all cases the thermocouple gauge gave an identical reading.

When the tests using one nozzle were completed, the other nozzle was substituted and the procedure repeated as before. The results noted are the average of three readings taken at each condition. The largest difference between two readings on the capacitance manometer at any particular condition amounted to 12 percent at most.

When the tests with the probe axes aligned with the nozzle centreline were completed, the probe with 8° wedge angle and 0.004 inch orifice height was yawed at 4° to the stream, i.e. with one side parallel to the flow, and readings of static and impact pressures noted for the range of conditions required. This is done to check the effect of using an asymmetric probe shape.

CHAPTER V

DISCUSSION

5.1 Theory and Previous Experiments

It has been clearly shown by all experimenters in this area of study that below Reynolds numbers of about 50, based on probe diameter, the inviscid equations of motion do not predict the impact pressures on a probe. The development of solutions to the problem using boundary layer theory are limited to a Reynolds number range of greater than 20. This is due to the basic assumption made in developing the equations that the boundary layer thickness remains thin with respect to the characteristic dimension of the body. However the results of Sherman [15] for a source shaped tube, and Homann [3] for a spherical probe agree to within 10 percent with the theoretical values of pressure coefficient for a sphere, down to a Reynolds number of 5. This is probably the limiting value of Reynolds number for which boundary layer theory will give useful results.

The characteristic dimension used in work with a circular cylinder placed transverse to the flow is the diameter of the cylinder. Treating the wedge as a two dimensional object of infinite width the characteristic dimension would be the height of the front face of the probe i.e. the orifice height. Basing the Reynolds number on this dimension the experiments are limited to a Reynolds number below 3 and boundary layer theory would not be expected to yield a valid solution in the range of these experiments.

Approaching the problem from the free molecular end it has been shown

by Chambré and Schaaf [10] that the important dimensions are the internal dimensions of the tubing which connects the gauge volume to the free stream. In order to analyze the problem free molecular flow must exist in this tubing. The criterion for this is that the Knudsen number must be greater than 1. However, in the experiments of Eukenhus [11] it appears that a Knudsen number of greater than 6 is required to ensure free molecular flow.

The minimum pressure on the probes being tested is 30 microns which corresponds to a mean free path of 0.065 inches. While this corresponds to a Knudsen number of 16 with respect to the orifice height of the smallest probes; it is not known to what extent the other dimensions, especially the probe width, will influence the onset of fully free molecular flow.

The probes will thus be in the transition regime at all times in the experiments and there is no satisfactory theoretical model for this regime. So far the only results for the transition regime are experimental ones. The results of Sherman [15] ranging from the continuum to the transition regime and the results of Pollard [2], for a similar probe, which cover the transition regime showed excellent agreement. The careful control of the experimental method and the repeatability of the results lead one to suppose that the relationship found by Pollard for such a probe is valid over the Reynolds number range from 3 to 30. This empirical relationship is used in the calibration of the nozzles.

5.2 Apparatus

The wind tunnel as it stands suffers from the disadvantage, from the point of view of this work, that there is no stagnation chamber up-

stream of the nozzle where a direct measurement of the total pressure can be made. With the 3 inch diameter nozzle the contraction ratio from the settling chamber to the nozzle throat is only 16:1 which is not sufficient to ensure zero velocity in the settling chamber. It is for this reason that the nozzles have to be calibrated with the flat-faced cylindrical probe.

The nozzles functioned adequately giving good agreement between the static pressure at the centreline and at the wall tap. The central core of uniform flow was wide enough to contain each probe tested. One problem which arises from using a probe 0.5 inches in diameter in a 3 inch diameter nozzle is that of the blockage effect. There is no literature on the subject of blockage in low density wind tunnels, nor on the problem of an object in the interface between an open and a closed tunnel as is the case at the nozzle exit section. However one can obtain an estimate of the blockage factor from subsonic wind tunnel data as given by Rogers [17]. The maximum blockage effect yields a drop of less than 0.5% in the static pressure reading and a rise of less than 1.5% in the value of the Mach number. Such small changes were neglected as they were within the magnitude of the error in measuring these two quantities.

In order to use the capacitance manometer, which is mounted outside the tunnel on the static pressure line, a length of about 3 feet of tubing was required between the wedge probe and the manometer. This length of tubing was expected to give a problem as the response time of such a length of tubing is quite long. In changing the pressure of the system by about 20 microns, by operating the butterfly valves, it was

found that the static pressure thermocouple gauge reached equilibrium in about 15 seconds while the capacitance manometer took about 1 minute to stabilize. This was found to be true with any of the probes on the impact pressure line and it is concluded that the response time of an orifice is much less than that of the connecting tubing.

All probes were connected to the impact pressure line by a 1/8 pipe tap connection to the supporting sting. To ensure that the top and bottom surfaces of each wedge probe were sealing adequately, the probes were broken down into their constituent parts and the seal examined, after the experiments had been performed. In each case the epoxy glue was seen to have sealed adequately and the orifice at the leading edge was the only opening between the tunnel and the impact pressure line.

The capacitance manometer was used to measure the difference between the impact and static pressure because better resolution of the pressure difference could be achieved than by using two thermocouple gauges. Consequently the velocity and viscous corrections can be more accurately determined. The thermocouple gauge is adequate to measure the static pressure as the resolution of this gauge is within 1 percent of the smallest reading used. For pressures below 30 microns another, more accurate means of measuring the static pressure is necessary.

When adjusting the air flowrate into the tunnel the metering valve was able to control the flowrate to within 0.1 mm of water on the Betz manometer used with the orifice meters.

5.3 Preliminary Calibrations

The thermocouple gauge calibration was carried out with and without

liquid nitrogen in the McLeod gauge cold trap. There was no distinguishable difference in results with liquid nitrogen cold trapping. The results are shown in Figure 8. This calibration is repeatable to within 2% over the range of 30 to 300 microns but below 30 microns the calibration is not so reliable. In the range 30 to 300 microns radiation effects on the thermocouple gauge should be negligible especially as the gauge is temperature compensated.

Both orifice meters were calibrated against the flowmeter kit and the results presented in Figures 9 and 10. In both cases the meters were seen to obey the general law that the flowrate is proportional to the square root of the pressure head across the orifice plate. Because of the small pressure head the effects of compressibility can be neglected.

The nozzle calibrations showed that the wall tap gave the nozzle static pressure to within 0.2 microns of the value recorded by the static pressure probe. This could be due to error in the capacitance manometer or to some small viscous effect to the static probe. In either case the error is negligible.

The check on the radial impact pressure gradient justifies the assumptions that the probes are in a central core of essentially uniform flow. Over a central core of radius 0.2 inches the maximum drop in impact pressure was 0.2 microns which amounts to a drop of less than 5 percent in the velocity across the core. The probe orifice is 0.375 inches wide and, allowing for error in positioning the probes, the probe will be in a constant velocity stream to within 5 percent.

The results of the calibration of the two nozzles for the Mach number on the centreline at a given flowrate and static pressure are given in Figures 11 and 12. The calibration is limited in that the maximum flowrate through the tunnel is limited to about 5.8 litres per minute at atmospheric pressure, and it is limited at low velocities and pressures in that the Reynolds number of the calibration probe has to be greater than 3 to use the viscous correction formula. The design of the nozzles and the pumping capacity of the booster pumps limits the maximum Mach number obtainable to about 0.45 in the larger nozzle. The maximum test Mach number was taken as 0.4 as this value could be reached over a pressure range from 30 to 160 microns.

The flowrate through the nozzle determines the Mach number at a particular static pressure. The flowrate could be controlled to within 0.1 mm of water on the Betz manometer which corresponds to a Mach number change of less than 1.3 percent.

5.4 Results on Wedge Probes

The calibration curves of the ratio of impact pressure to total pressure versus the Reynolds number, based on the probe orifice height, are given for each probe tested in Figures 13 to 19. These curves are for the case of the probe axis aligned with the flow direction.

The results, Figures 13-16, show that the viscous correction increases as the orifice height is reduced. With the 0.004 inch orifice height, Reynolds numbers of 0.024 were reached but, even at this low value, the free molecular limit was not approached. From the results obtained it cannot be seen where the free molecular limit begins and it

must be concluded that the width of the probe orifice has a considerable effect on retarding the onset of free molecular flow. At the other end of the transition regime the results for the 0.108 inch orifice height show a definite trend to approach the inviscid continuum value for the impact pressure. At Reynolds numbers greater than 5 for flow Mach numbers of less than 0.4 the error in ignoring the viscous effect is less than 3 percent. For all probes the correction was positive, and negative corrections as noted in [4], [13], and [15] were not encountered. The probes with 0.013 and 0.014 inch orifice heights gave viscous corrections between those of the largest and smallest probes.

It is desirable to have one characteristic dimension for calculating Reynolds numbers which will correlate the results of all the probes with the same wedge angle. Various combinations of the dimensions of the probes were tried in order to find this dimension. The dimension which most successfully correlated the results was the equivalent diameter of the orifice defined by, $D = (\text{orifice area} \times 4/\pi)^{1/2}$. Figures 20 and 21 show the viscous corrections for all four probes with a wedge angle of 8° together with the results given by Pollard [2] for a round probe plotted against the Reynolds number based on the equivalent diameter.

The results show that the equivalent diameter can correlate the data with a fair degree of success. At a Mach number of 0.4 there is the greatest amount of scatter in the results especially between the data of the probes with orifice heights 0.108 inches and 0.042 inches, with the smaller probe giving larger corrections. This trend can be seen in all four curves drawn in Figures 20 and 21.

The experimental results agree fairly well with the results given by Pollard [2] for a round probe, basing the Reynolds number on the probe diameter. As the response time of a probe will depend to some extent on the area of the probe orifice one may expect from these results that a wedge probe would have a response time of the same order of that of a round probe with the same orifice area. The response times of the probes could not be determined accurately in this experiment due to the length of the impact pressure line.

The effect of a change in orifice height on the 8° wedge probe is presented in another form in Figure 22. This Figure compares the results of wedge probes with those of a flat-faced cylindrical probe of diameter equal to the wedge probe orifice height. It can be seen that the wedge probe gives a much lower pressure correction than the cylinder for a given Reynolds number. This is in agreement with MacMillan's results [4] where flattened tubes had lower viscous corrections than the circular cylinder tubes, the correction dropping as the width to height ratio was increased. This lowering of the viscous correction as a body becomes more two dimensional is in qualitative agreement with the theoretical and experimental results of Homann [3] who showed that the correction to a cylinder transverse to the flow is less than that on a spherical probe.

This result can be used to great advantage when velocity readings are required with small spatial resolution, as in measuring the velocities in the boundary layer. The wedge probe with orifice height h will give a much smaller viscous correction than a circular cylinder probe of diameter h. The viscous correction to the wedge probe may become

negligible which would considerably simplify the reduction of data from such impact pressure readings.

MacMillan [4] noted that his flattened probes with width to height ratios of 7 and 11 gave very similar viscous corrections. No such result was observed in this set of experiments with wedge probes. The width to height ratios of the orifices used were 3.74, 8.93, 28.9 and 93.8.

An attempt was made to find an empirical relationship between the ratio of impact to total pressure and the ratio of Mach number to Reynolds number, as had been found by Pollard for cylindrical probes for Reynolds numbers greater than 3. Figure 23 shows such a relationship for the 8° wedge probe with an orifice height of 0.108 inches for points with a Reynolds number, based on the orifice height of greater than 1.2. The relationship is $P_I/P_o = 0.99 + 0.53\ M/Re_h$.

This relationship suggests that in the limit as one reaches high Reynolds numbers the impact pressure becomes lower than the total pressure. It is therefore doubtful if the relationship can be extrapolated outside the range of Reynolds numbers tested.

A linear relationship, such as this, could not be found for any of the other wedge probes tested. The reason for this could be that only the largest wedge probe came close enough to the continuum regime to act thus. This is in agreement with Pollard's [2] results as they also are only valid close to the continuum regime.

The effects of changing the wedge angle on a probe with an orifice height of 0.004 inches is shown in Figures 13, 17, 18, 19. This shows that the viscous effect decreases as the wedge angle is increased. This

result could be explained from a continuum approach by noting that such an angle increase tends to make the nose of the probe more blunt and the effective radius of curvature of the nose would be increased. If this is an important dimension of the probe, the Reynolds number of the probe will rise as the angle is increased which would give a lowering of the impact pressure.

In an attempt to examine the effect of the angle change on the viscous correction the values of $P_I - P_o$ were found for each condition of static pressure and Mach number. The ratios of $P_I - P_o$ for each probe to $P_I - P_o$ for the 8° wedge probe, under the same nozzle conditions, was calculated. Although there is a fair amount of scatter in the results, no discernable trend in this viscous correction ratio could be found with either the pressure or the Mach number of the stream. The statistical average and standard deviation of the viscous correction ratio were then calculated from the data for each probe and these results are presented in Figure 24. This curve shows the definite trend in the readings for the viscous correction to decrease as the angle increases. With a standard deviation of approximately 3% of the mean value for all the probes the results are fairly consistent bearing in mind the scatter in the original data.

By increasing the wedge angle by a factor of 4, from 8° to 32° the corresponding average drop in viscous correction is about 20%. This effect does not appear to be very useful as, to gain this small drop in viscous correction, the probe size must be increased drastically. This bulkier probe can be expected to give rise to a blockage problem and the corresponding internal dimensions could be expected to give a larger response time.

The results from the test on the 8° wedge angle probe with a 0.004 inch orifice yawed at an angle of 4° to the free stream were not plotted as they are substantially the same as in the case of the same probe at 0° yaw. This can be seen clearly from the table of results, Appendix A. The difference in viscous correction between the two sets of results was never more than 7.6 percent.

From this test it can be seen that a yaw angle of 4° on the 8° wedge probe gives no appreciable change in impact pressure. This allows the probe calibration to be used when the probe has one side parallel to the flow direction. This is of use when measuring the boundary layer on a flat plate as the probe orifice can be moved right up to the plate surface.

The scatter in the data of the above test is of the same magnitude as that obtained in comparing the effect of wedge angle. This ± 8 percent reflects the accuracy with which the viscous correction can be determined with this particular setup. There is therefore some room for improvement in the calibration of these wedge probes. Having to set up the same conditions of static pressure and flowrate for each probe tested undoubtedly leads to error when the exact values are not reproduced. This error could be overcome by setting up the flow conditions once and then inserting the probes into the flow in turn. This involves some problems in transferring the impact pressure line to each probe in turn. A stagnation chamber, where the total pressure can be measured, would enable an absolute calibration to be made and any errors involved in using a calibration probe could be removed.

CHAPTER VI

CONCLUSIONS

Wedge probes were calibrated to show viscous corrections for a range of pressures from 30 to 280 microns and for a range of Mach numbers from 0.1 to 0.4 in air. The results are plotted as a function of the Reynolds number, based on the orifice height.

The viscous correction decreases as the Reynolds number increases, as expected. In the Reynolds number range of the tests the probes were never in the free molecular regime nor in the inviscid continuum regime, although the results for the probe with the largest orifice height appears to approach this latter limit.

The viscous corrections to the 8° wedge probes were correlated by the Reynolds number based on the equivalent diameter of the probe orifice. The results, when plotted thus, agree with results given by Pollard [2] for flat-faced circular cylinder probes.

The viscous correction to wedge probes with a particular orifice height has been shown to be substantially less than that for a flat-faced cylindrical probe of a diameter equal to this orifice height. This result is of use in taking velocity readings where small spatial resolution is required, as in boundary layer measurements for example.

An increase in the probe wedge angle was found to cause a decrease in the viscous correction. Due to the scatter in results the exact nature of this relationship could not be determined but a trend does exist.

No change in viscous correction was found on an 8° wedge probe with a 0.004 inch high orifice when the probe was yawed through 4°. Thus such

a probe, when placed with one side parallel to the flow, as in boundary layer measurements, will have the calibration given in Figure 13.

The wedge probe has some distinct advantages over flat-faced, cylindrical probes when measuring flow velocities at low Reynolds numbers. This thesis provides the calibrations for some wedge probes over a limited range of Mach numbers and Reynolds numbers.

In order to achieve better results it is recommended that some method of introducing several probes into a fixed, uniform stream be developed. Also a stagnation chamber, where total pressure could be read would be useful.

Tests over a wider range of Reynolds number and probe geometry would be useful in that it would be helpful if the entire transition regime could be covered.

BIBLIOGRAPHY

1. Barker, M., "On the Use of Very Small Pitot Tubes for Measuring Wind Velocity", Proceedings of the Royal Society, Series A, Vol. 101, 1922, pp. 435-445.

2. Pollard, M.G., "Interpretation of Impact Pressures in Rarefied Gas Flows", Rarefied Gas Dynamics, Vol. 1, 1968, pp. 811-834.

3. Homann, G., "The Effect of High Viscosity on the Flow Around a Cylinder and Around a Sphere", NACA TM 1334, 1952.

4. MacMillan, F.A., "Viscous Effects on Flattened Pitot Tubes at Low Speeds", Journal of the Royal Aeronautical Society, Vol. 58, 1954, pp. 837-839.

5. Berard, G.P., "The Transition Boundary Layer Near the Leading Edge", Ph.D. Thesis, University of Alberta, 1970.

6. Schlichting, H., "Boundary Layer Theory", McGraw-Hill, New York, 1968.

7. Owczarek, J.A., "Fundamentals of Gas Dynamics", International Textbook Company, Pennsylvania, 1968.

8. Chambré, P.L., "The Theory of the Impact Tube in a Viscous Compressible Gas", University of California, Institute of Engineering Research, Report No. HE-150-50, 1948.

9. Chambré, P.L., "The Impact Tube in a Viscous Compressible Gas", University of California, Institute of Engineering Research, Report No. HE-150-63, 1948.

10. Chambré, P.L., and Schaaf, S.A., "The Theory of the Impact Tube at Low Pressures", Journal of the Aeronautical Sciences, Vol. 15, No. 12, 1948, pp. 735-737.

11. Enkenhus, K.R., "Pressure Probes at Very Low Density", University of Toronto, Institute of Aerophysics, UTIA Report No. 43, 1957.

12. Dushman, S., "Scientific Foundations of Vacuum Technique", John Wiley, New York, 1949.

13. Hurd, C.W., Chesky, C.W. and Shapiro, A.H., "Influence of Viscous Effects on Impact Tubes", Journal of Applied Mechanics, Vol. 20, No. 2, 1953, pp. 253-256.

14. MacMillan, F.A., "Viscous Effects on Pitot Tubes at Low Speeds", Journal of the Royal Aeronautical Society, Vol. 58, 1954, pp. 570-574.

15. Sherman, F.S., "New Experiments on Impact Pressure Interpreation in Supersonic and Subsonic Rarefied Air Streams", NACA TN 2995, 1953.

16. Merriam, K.G. and Spaulding, E.R., "Comparative Tests of Pitot-Static Tubes", NACA TN 546, 1935.

17. Rogers, E.W.E., "Blockage Effects in Closed or Open Tunnels", AGARD-ograph 109, "Subsonic Wind Tunnel Wall Corrections", Ed. Garner, H.C., 1966, pp. 279-340.

APPENDIX A

EXPERIMENTAL DATA

DATA

IMPACT PRESSURES ON ALL PROBES AT MACH NOS.

AND STATIC PRESSURES GIVEN

(Pressure in Microns)

ORIFICE HEIGHT-INS.		0.004	0.013	0.042	0.108	0.004	0.004	0.004	0.004*
WEDGE ANGLE-DEG.		8.0	8.0	8.0	8.0	16.0	24.0	32.0	8.0
PS	M	PI	PI	PI	PI	PI	PI	PI	PI
280.0	0.10	300.70	295.00	290.85	286.35	299.70	298.10	296.95	299.35
280.0	0.15	307.55	299.40	294.65	289.00	306.55	303.90	302.60	
280.0	0.20	314.80	305.15	299.40	291.70	314.30	311.15	309.65	314.90
260.0	0.10	281.55	275.05	271.00	266.35	279.80	278.25	277.80	283.00
260.0	0.15	286.15	278.70	274.00	268.45	284.80	282.60	281.30	
260.0	0.20	293.70	284.50	278.90	271.20	293.20	290.10	288.70	293.05
260.0	0.25	302.60	290.40	284.75	275.40	302.10	298.95	297.35	
240.0	0.10	260.00	254.65	251.00	246.25	259.55	258.00	256.65	259.90
240.0	0.15	266.00	258.50	254.00	248.30	264.60	262.80	261.05	
240.0	0.20	272.80	263.65	258.35	250.70	272.45	269.10	267.90	271.60
240.0	0.25	280.30	269.80	263.10	254.10	280.00	276.30	274.75	
220.0	0.10	239.65	234.00	230.65	226.05	238.85	237.20	236.20	240.85
220.0	0.15	244.70	238.10	233.65	228.05	243.70	241.80	240.80	
220.0	0.20	251.60	243.40	237.90	230.65	251.00	247.85	246.75	250.30
220.0	0.25	259.15	249.05	242.65	233.80	258.85	255.20	253.40	
220.0	0.30	270.20	255.70	249.70	238.50	269.65	264.95	263.80	269.25
200.0	0.10	218.20	213.90	210.65	206.20	218.30	216.70	215.80	216.95
200.0	0.15	224.00	217.70	213.55	207.90	223.50	221.65	220.70	
200.0	0.20	230.65	222.75	217.50	210.40	229.50	227.00	225.50	232.00
200.0	0.25	238.35	228.15	222.10	213.25	237.15	234.00	232.45	
200.0	0.30	245.55	234.30	227.20	216.70	244.85	240.85	239.35	246.85

PS	M	PI	PI	PI	PI	PI	PI	PI	PI
180.0	0.10	198.65	193.45	190.60	186.00	198.05	196.20	195.20	199.25
180.0	0.15	203.65	197.25	193.35	187.75	202.50	200.50	199.40	
180.0	0.20	208.50	201.50	196.50	189.80	207.60	205.45	203.90	208.65
180.0	0.25	216.35	207.10	200.75	192.90	214.80	211.35	210.50	
180.0	0.30	223.60	212.90	206.00	196.00	223.05	219.00	217.65	223.70
180.0	0.35	231.05	219.05	211.15	199.50	231.05	226.20	224.50	
160.0	0.10	178.00	173.00	170.25	165.80	177.10	175.40	174.35	177.60
160.0	0.15	181.80	176.80	173.00	167.65	181.15	179.40	178.45	
160.0	0.20	188.00	181.15	176.40	169.50	187.10	184.55	182.95	187.65
160.0	0.25	193.45	185.85	179.80	172.00	192.60	189.70	188.25	
160.0	0.30	201.25	191.40	184.60	175.20	199.95	196.00	194.90	202.80
160.0	0.35	209.30	197.30	190.00	178.55	208.15	203.70	201.60	
160.0	0.40	217.80	203.60	196.10	182.65	216.95	211.45	210.05	219.30
140.0	0.10	156.90	153.10	150.50	145.95	157.00	155.35	154.45	155.80
140.0	0.15	150.40	156.10	152.60	147.20	160.50	158.35	157.35	
140.0	0.20	165.55	159.50	156.60	149.15	164.50	162.50	161.40	165.75
140.0	0.25	174.05	165.00	159.25	151.55	170.60	168.20	167.45	
140.0	0.30	178.70	169.90	163.00	154.40	177.15	173.85	172.00	177.45
140.0	0.35	185.80	174.70	168.00	157.50	184.65	180.00	178.85	
140.0	0.40	192.85	180.45	172.90	160.80	191.90	187.05	185.60	192.70
120.0	0.10	135.90	132.70	130.10	125.60	135.15	134.35	133.35	136.35
120.0	0.15	139.40	135.00	132.15	126.90	138.95	137.20	135.95	
120.0	0.20	143.20	138.10	134.65	128.60	143.10	140.60	139.55	144.50
120.0	0.25	149.55	142.75	138.00	130.95	148.20	145.75	144.65	
120.0	0.30	155.70	149.05	142.20	133.55	154.20	151.90	151.10	156.95
120.0	0.35	161.55	152.65	145.95	136.25	159.85	156.80	155.10	
120.0	0.40	168.50	158.35	150.50	139.35	167.35	162.35	161.25	169.15

PS	M	PI	PI	PI	PI	PI	PI	PI	PI
100.0	0.10	115.30	112.50	109.85	105.90	114.80	113.80	112.55	115.00
100.0	0.15	117.90	114.85	111.70	107.00	117.50	116.20	114.85	
100.0	0.20	120.75	117.75	113.70	108.60	120.30	119.00	117.75	121.30
100.0	0.25	125.55	120.35	116.50	109.85	125.75	122.70	121.45	
100.0	0.30	132.05	124.95	120.20	112.55	130.65	127.90	127.05	130.65
100.0	0.35	139.20	130.30	124.05	114.80	136.95	133.50	132.20	
100.0	0.40	143.35	134.40	127.30	117.50	142.55	137.95	136.90	143.35
90.0	0.10	104.35	102.05	99.35	95.70	103.95	102.95	101.75	104.20
90.0	0.15	107.35	104.50	101.25	97.00	106.90	105.55	104.20	
90.0	0.20	109.85	106.85	103.20	98.20	109.60	108.10	106.80	110.80
90.0	0.25	113.90	109.55	105.80	99.50	113.80	111.35	110.35	
90.0	0.30	119.20	113.45	109.25	101.60	118.75	116.00	114.95	120.20
90.0	0.35	126.10	118.15	112.55	104.00	123.95	121.00	119.90	
90.0	0.40	133.00	123.30	116.70	106.80	129.80	126.65	125.60	131.30
80.0	0.10	93.65	91.40	89.50	85.45	93.30	92.45	91.40	94.40
80.0	0.15	96.50	93.80	91.00	86.80	95.80	94.70	93.65	
80.0	0.20	99.35	96.45	93.05	88.15	98.75	97.55	96.10	99.35
80.0	0.25	102.30	99.45	95.30	89.70	101.70	100.30	98.75	
80.0	0.30	107.15	101.90	98.00	90.95	106.60	103.85	102.80	107.15
80.0	0.35	112.75	106.20	101.40	93.40	111.40	108.55	107.70	
80.0	0.40	118.35	110.65	104.40	95.95	116.70	113.40	112.50	116.65
70.0	0.15	85.65	82.00	80.25	76.10	84.60	83.85	82.65	
70.0	0.20	87.90	85.00	81.95	77.65	86.90	85.95	84.35	87.90
70.0	0.25	90.75	87.85	84.40	79.35	90.20	88.85	87.10	
70.0	0.30	94.15	91.30	87.00	80.85	93.55	91.95	90.25	94.30
70.0	0.35	98.65	93.30	89.70	82.40	98.45	95.55	94.55	
70.0	0.40	104.00	97.70	93.10	84.60	103.30	100.00	99.10	102.50

PS	M	PI	PI	PI	PI	PI	PI	PI	PI
60.0	0.15	73.95	70.85	69.45	65.75	73.20	72.35	71.45	
60.0	0.20	76.00	73.80	72.05	67.25	75.75	74.65	73.60	76.85
60.0	0.25	79.30	76.80	73.45	68.80	78.20	77.35	75.70	
60.0	0.30	82.50	79.45	76.05	70.45	81.60	80.10	78.60	82.30
60.0	0.35	85.75	82.50	78.60	72.00	84.75	83.50	81.60	
60.0	0.40	90.70	87.00	81.60	74.55	89.85	87.90	86.05	90.50
50.0	0.20	64.40	62.30	61.00	56.90	63.90	62.80	62.10	65.30
50.0	0.25	66.60	64.50	62.80	57.85	66.00	65.00	63.95	
50.0	0.30	69.15	67.00	63.85	59.20	68.75	67.50	66.00	70.00
50.0	0.35	72.05	69.60	66.10	60.85	71.30	69.85	68.45	
50.0	0.40	75.75	72.65	68.60	62.65	74.75	73.00	71.55	76.15
40.0	0.25	54.70	52.90	51.60	47.45	54.10	53.35	52.15	
40.0	0.30	56.55	54.75	52.95	48.40	55.80	55.10	53.90	57.55
40.0	0.35	58.50	56.45	54.80	49.40	57.95	57.00	55.70	
40.0	0.40	61.20	59.20	56.00	51.05	60.30	59.50	57.70	61.55
30.0	0.30	43.65	42.35	41.50	37.50	43.15	42.65	41.40	44.45
30.0	0.35	45.25	44.00	42.85	38.60	44.90	44.05	42.90	
30.0	0.40	47.30	45.80	44.45	39.55	46.85	46.05	44.60	48.30

* Yawed at 4°

FIGURES

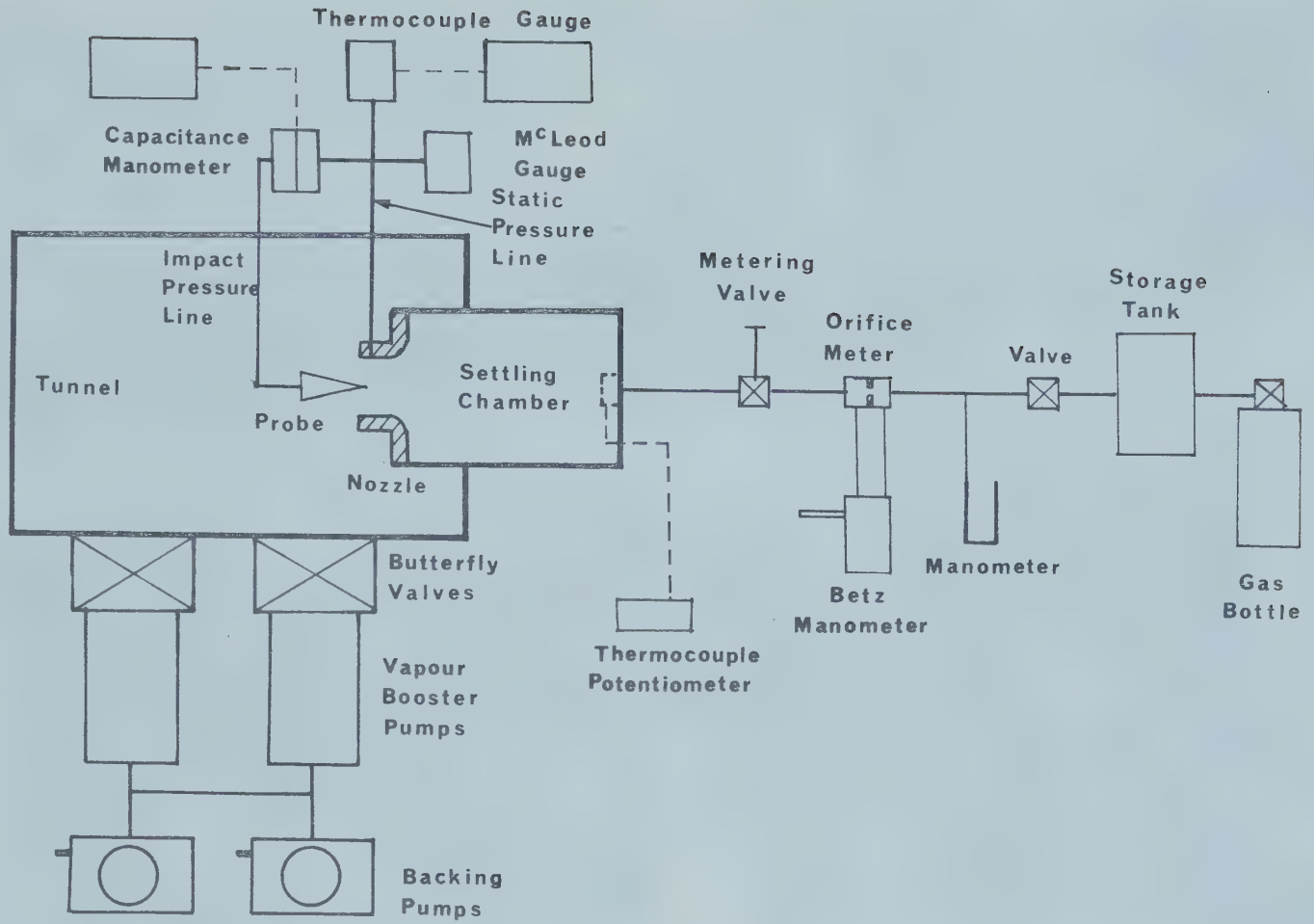

FIGURE 1. Schematic Layout of the Low Density Wind Tunnel

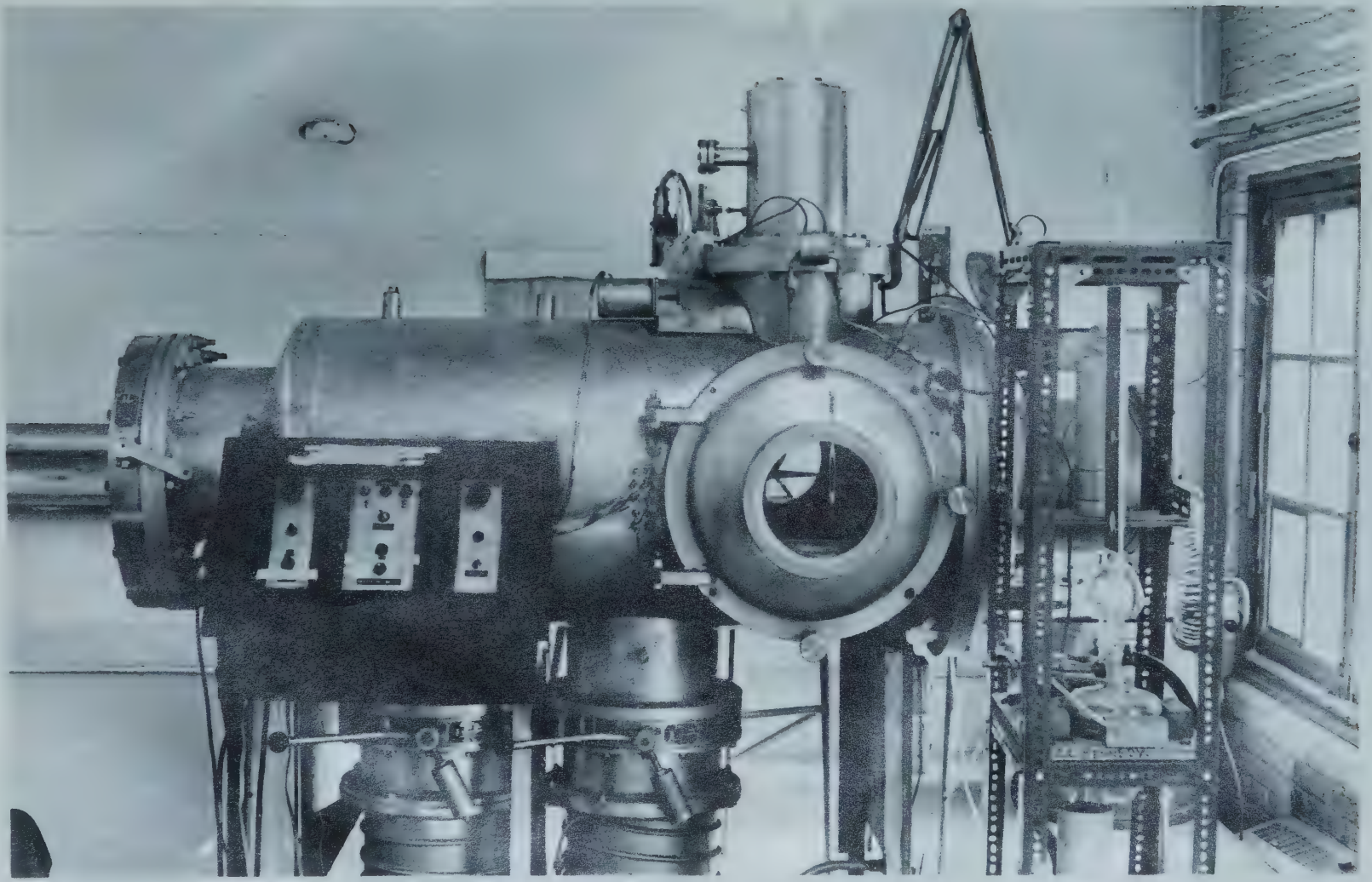

FIGURE 2. Photograph of Low Density Wind Tunnel

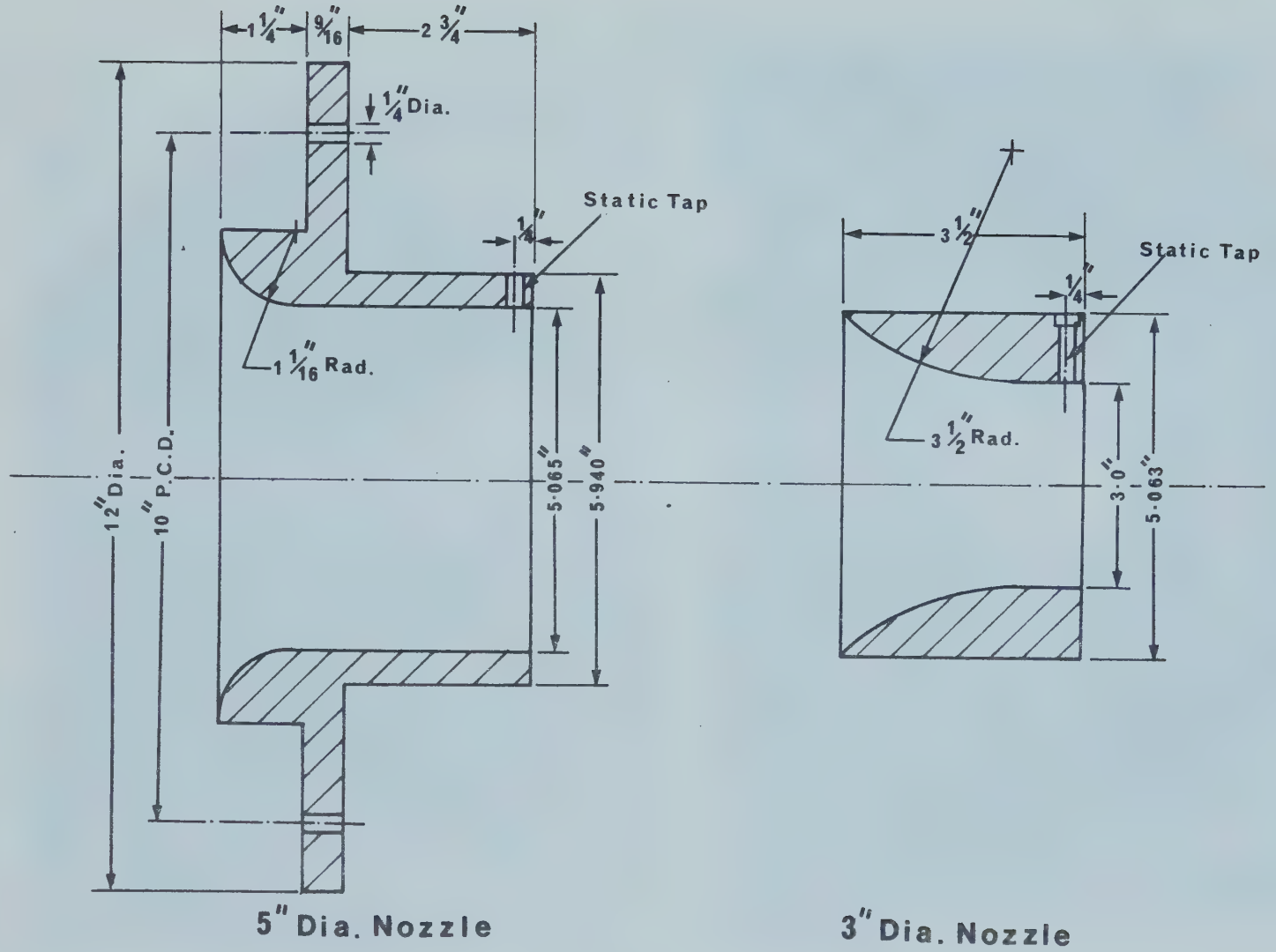

FIGURE 3. Schematic Drawing of the Nozzles

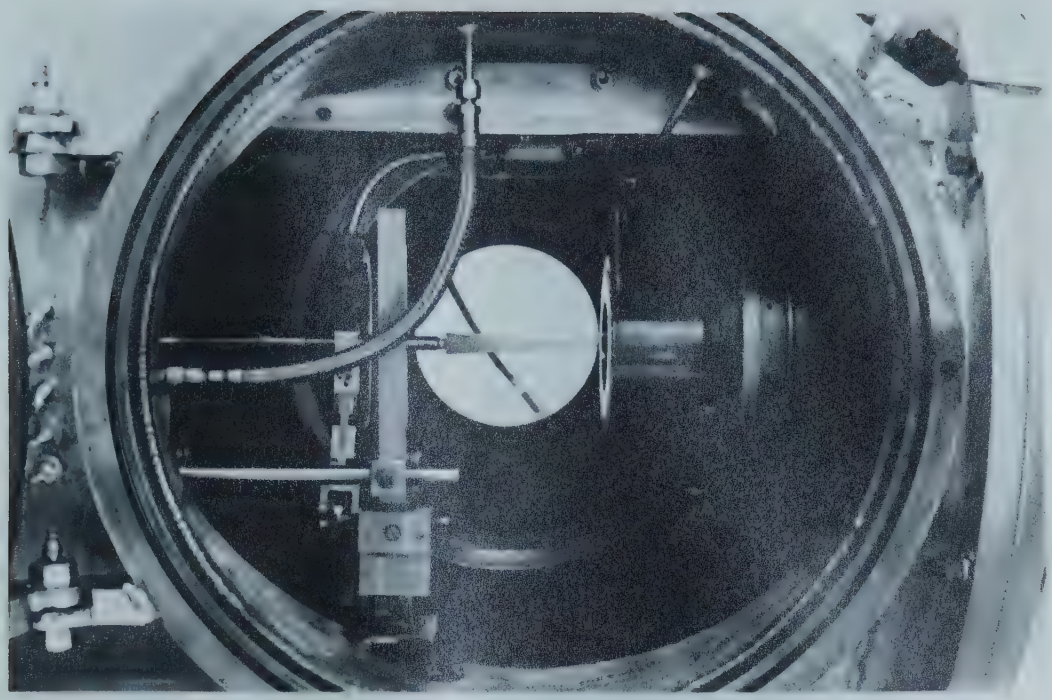

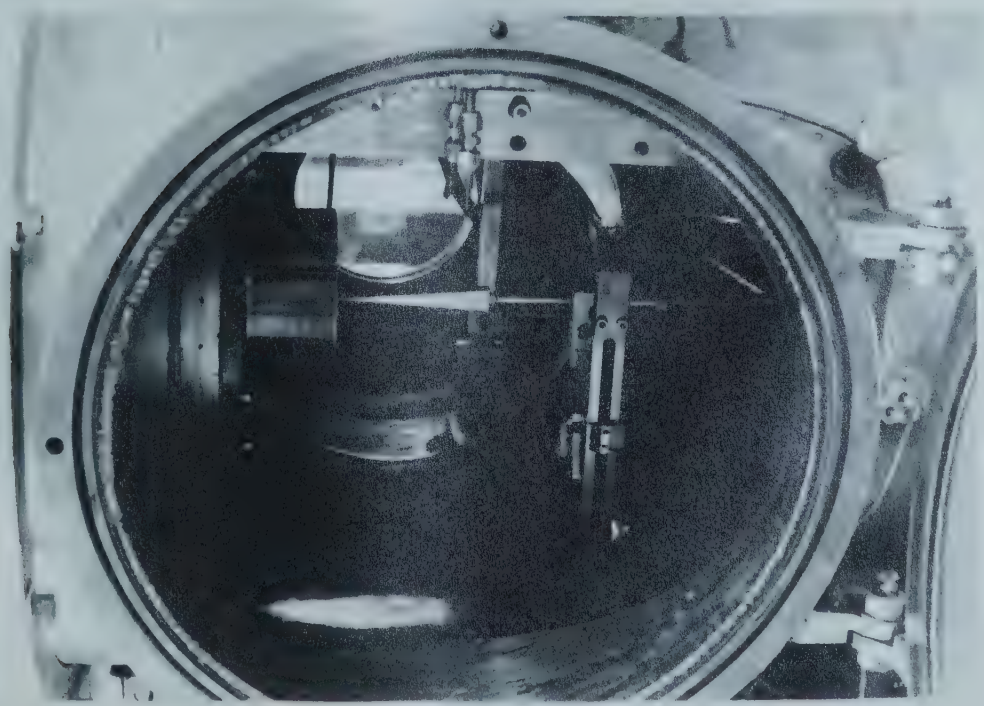

FIGURE 4. Photographs of Test Section

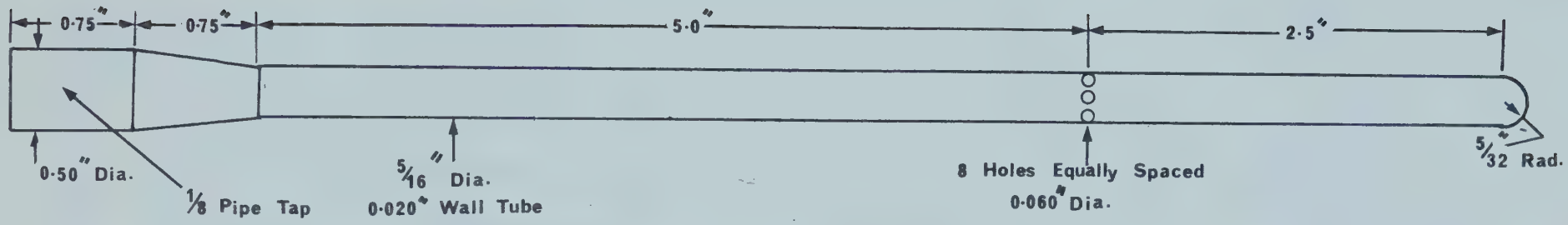

Static Pressure Probe

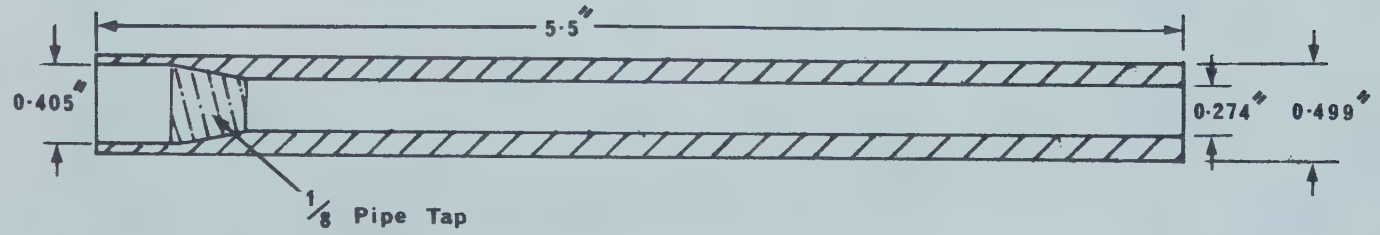

Impact Pressure Calibration Probe

FIGURE 5. The Static Pressure and Impact Pressure Calibration Probes

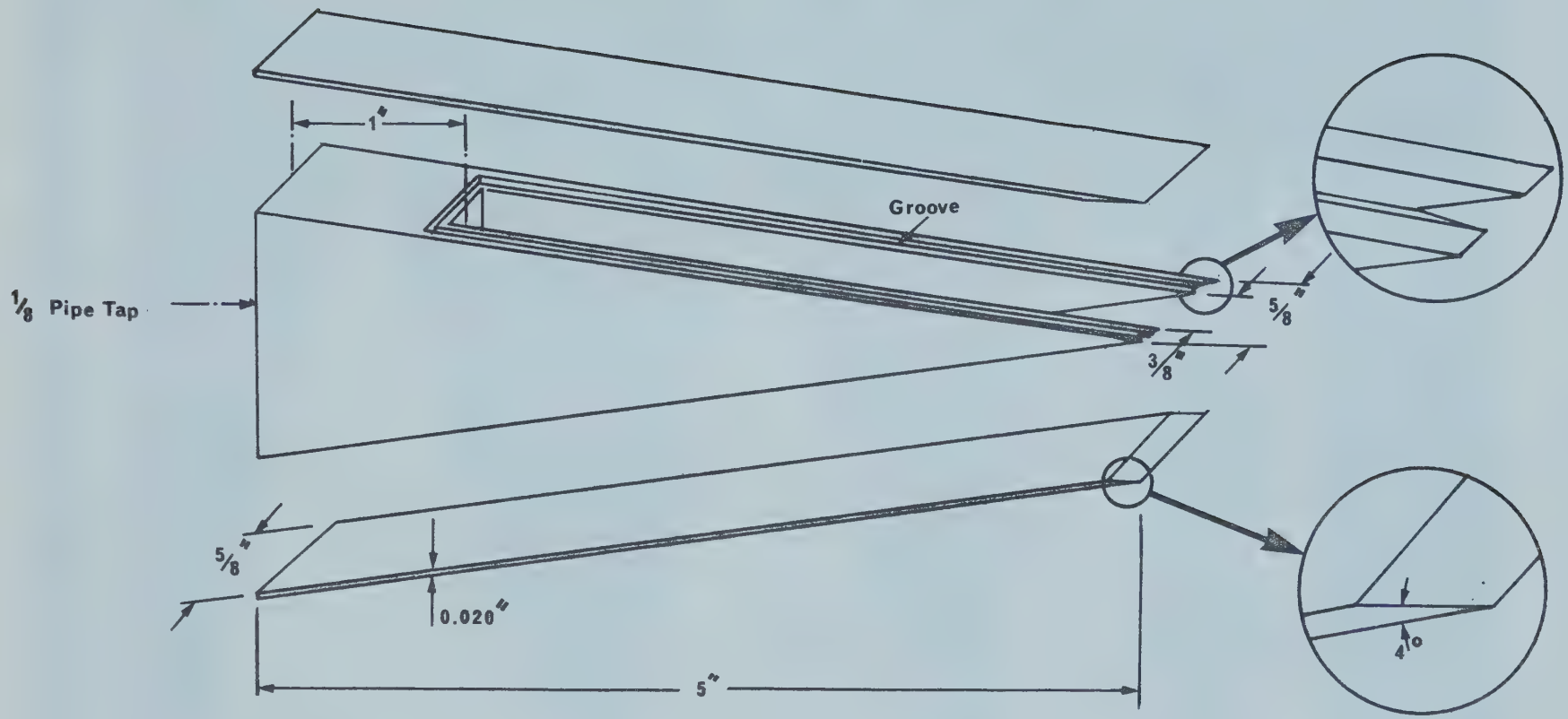

FIGURE 6. Exploded Drawing of Wedge Probe

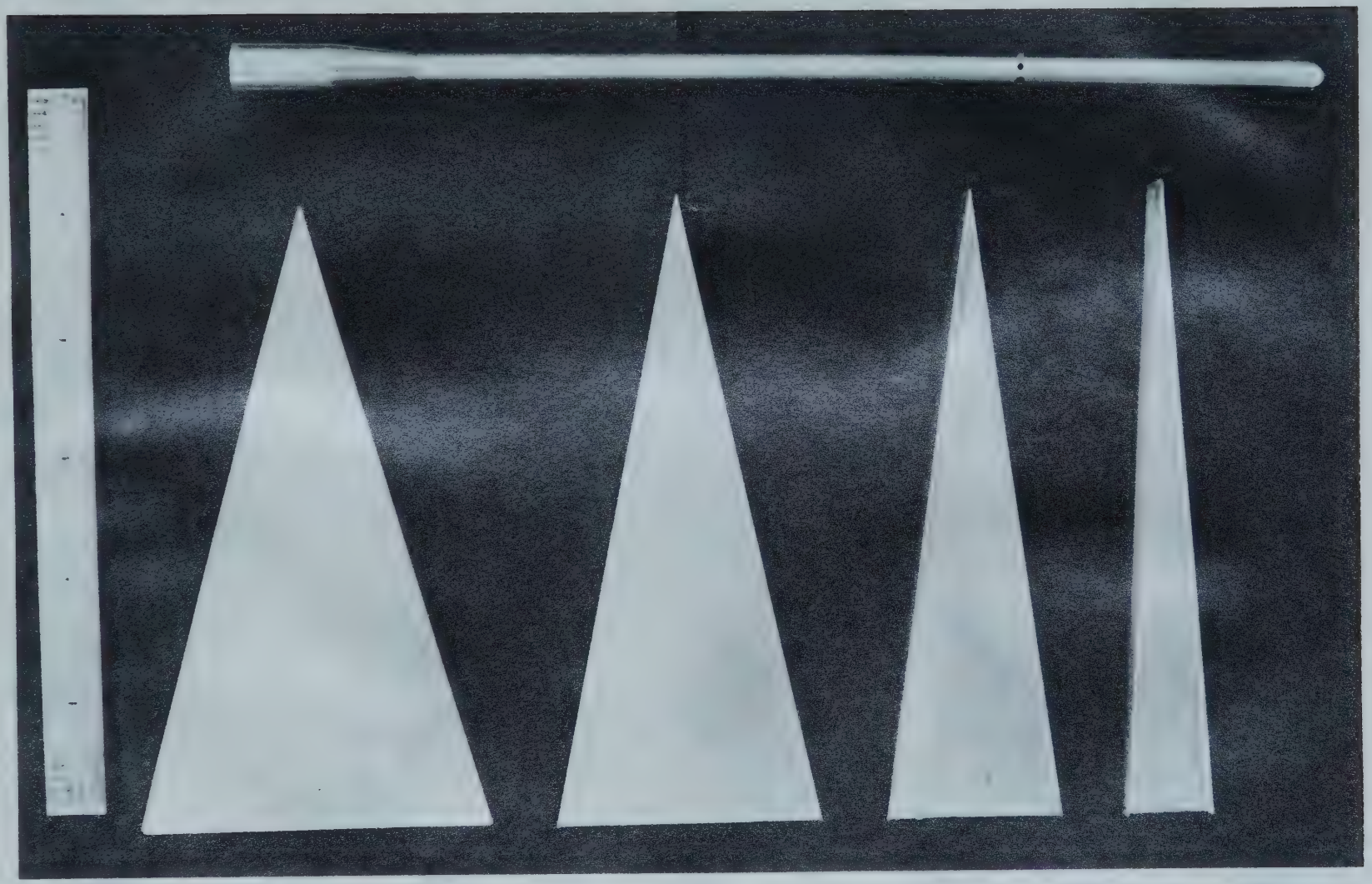

FIGURE 7. Photograph of Probes

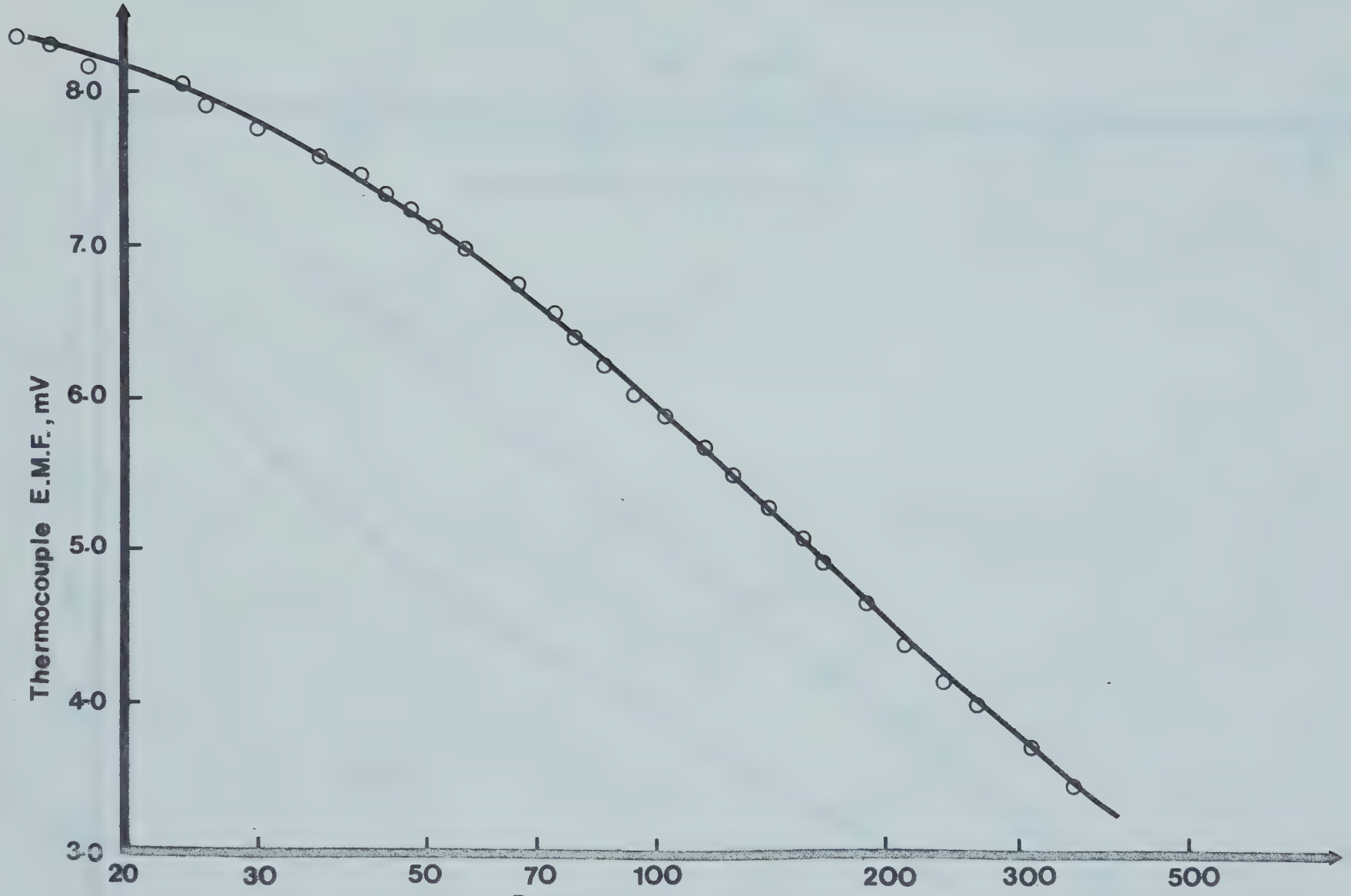

FIGURE 8. Thermocouple Gauge Calibration Curve

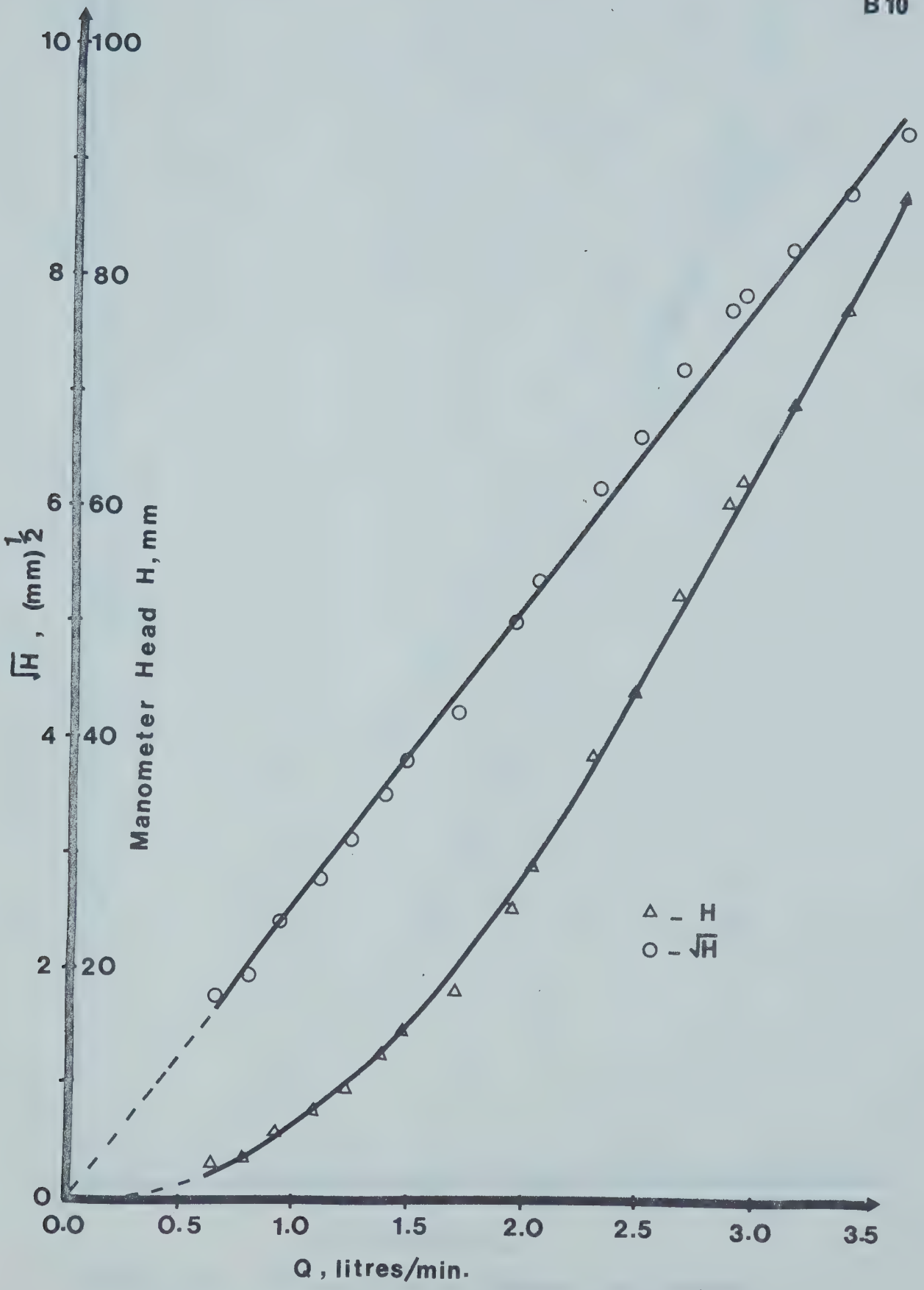

FIGURE 9. $\frac{1}{8}$ Inch Orifice Meter Calibration

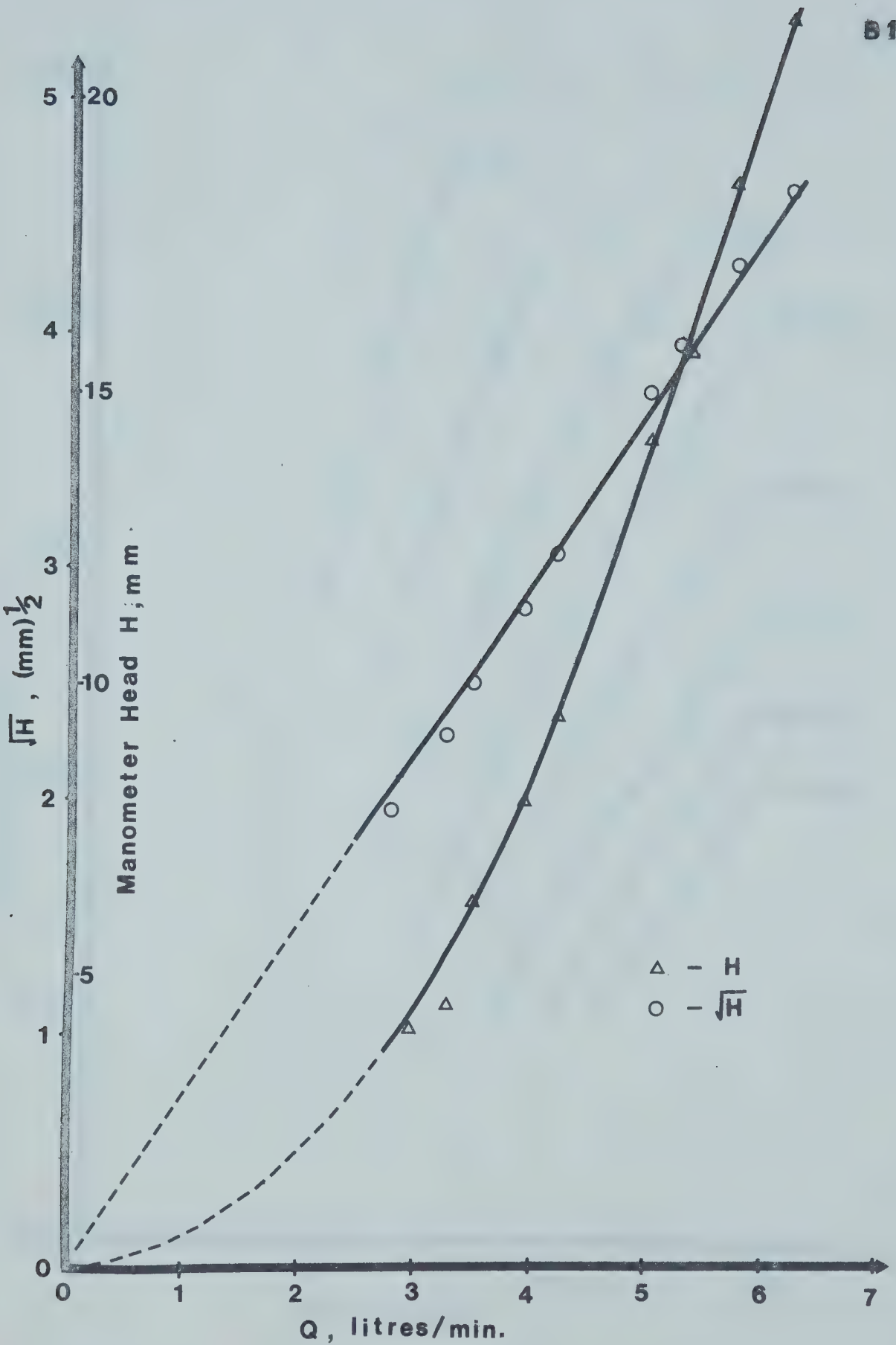

FIGURE 10. ¼ Inch Orfice Meter Calibration

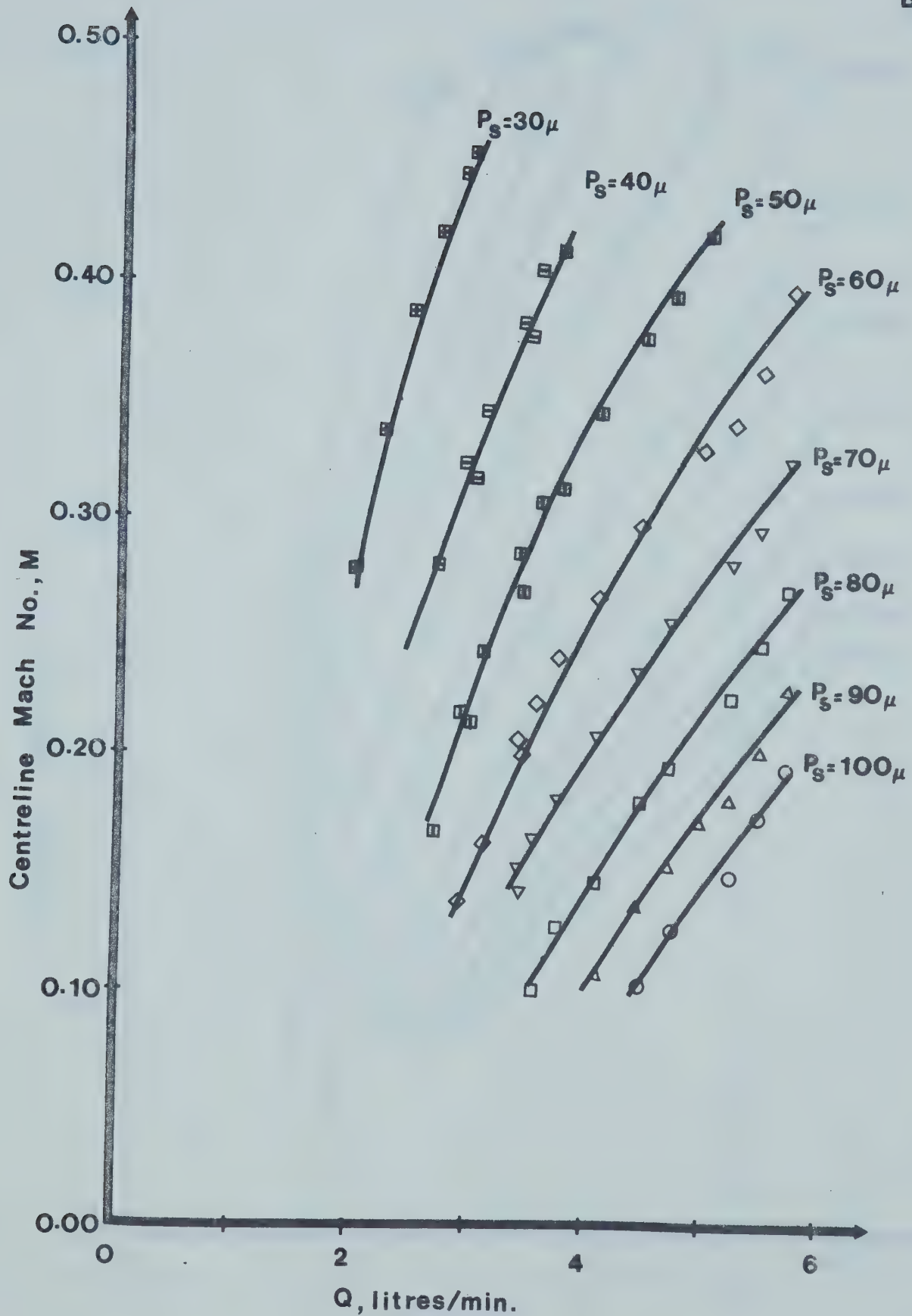

FIGURE 11. 5 Inch Nozzle Calibration Curves

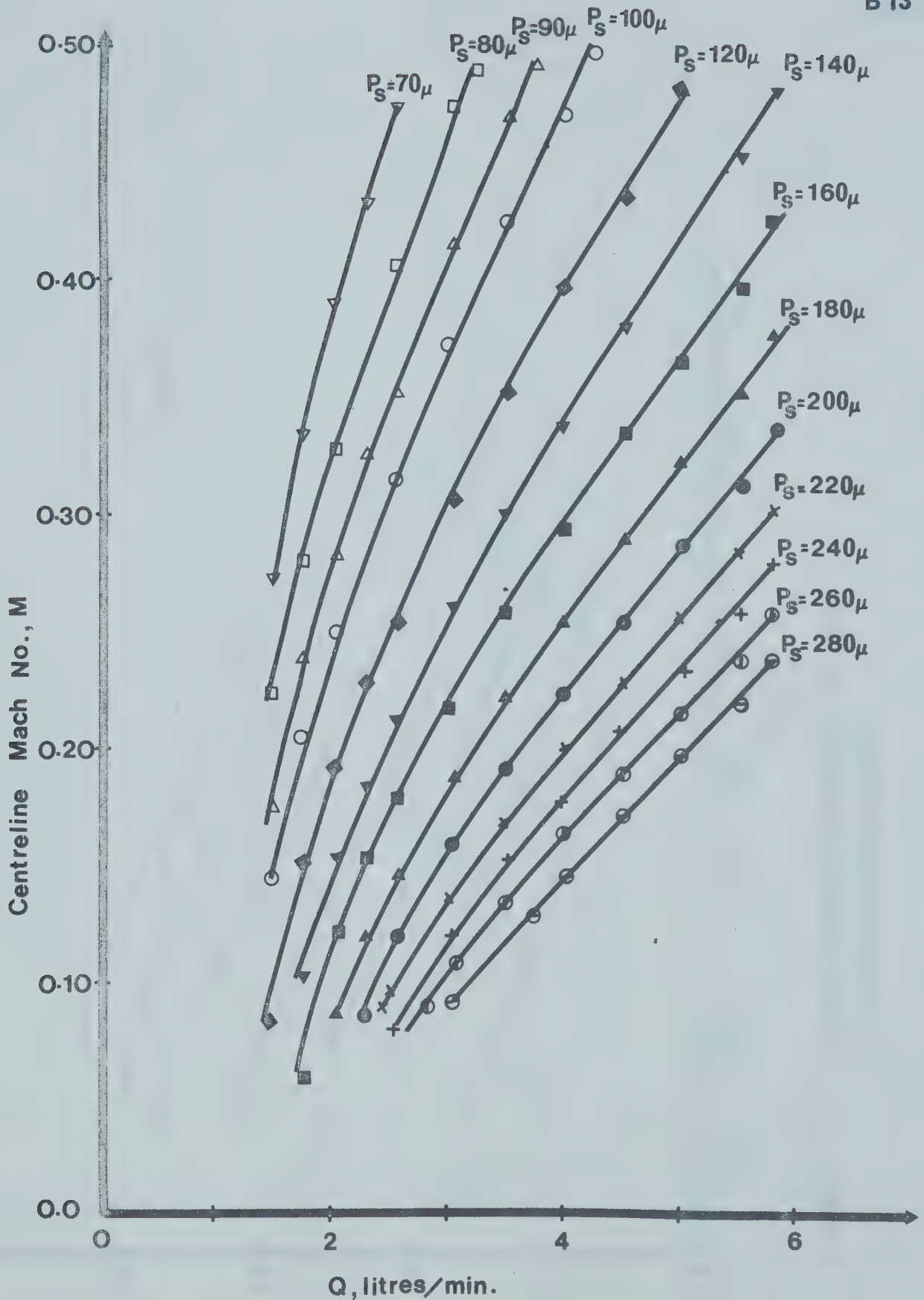

FIGURE 12 . 3 Inch Nozzle Calibration Curves

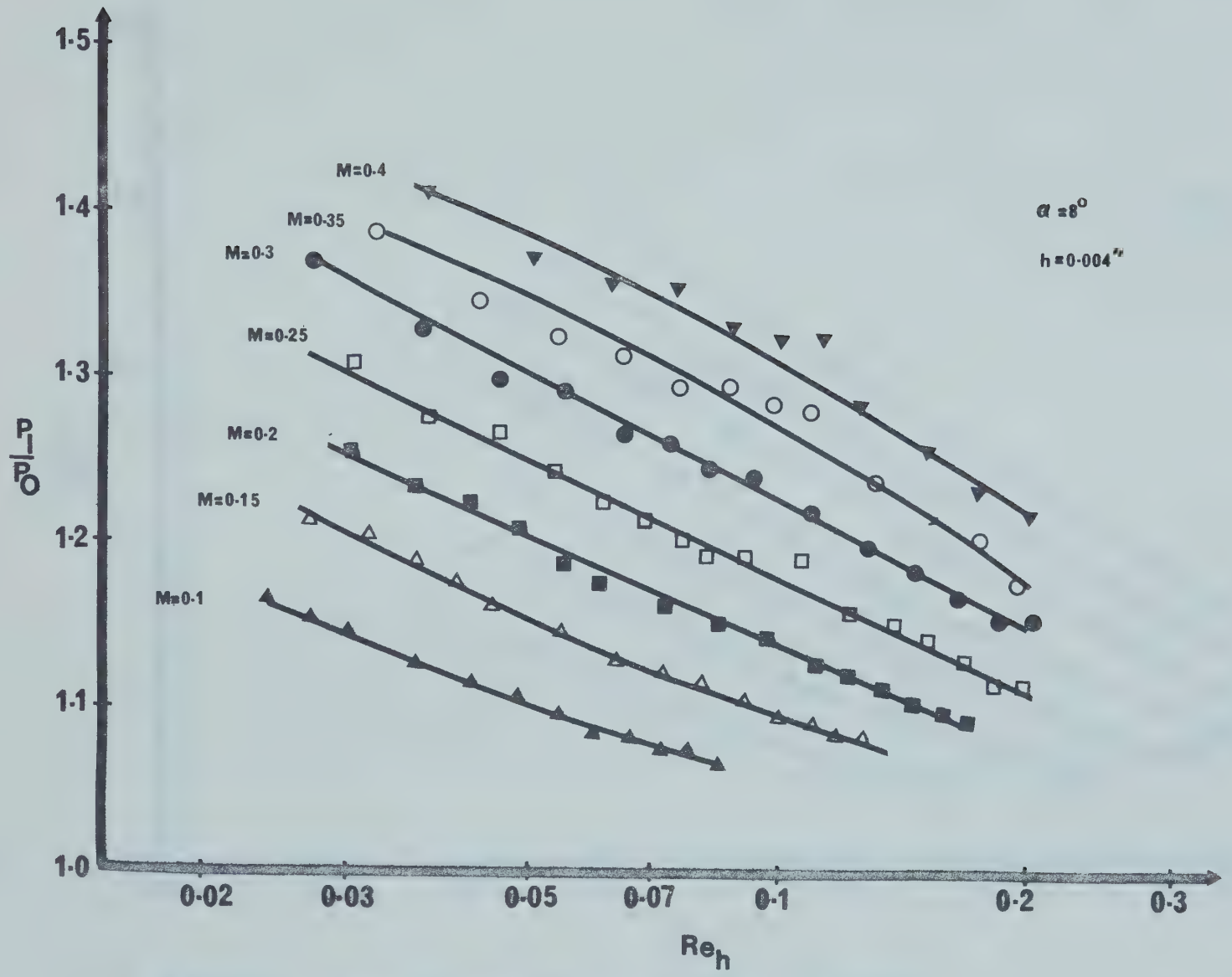

FIGURE 13. Wedge Probe Correction Factors; 8° Wedge, h=0·004 inches

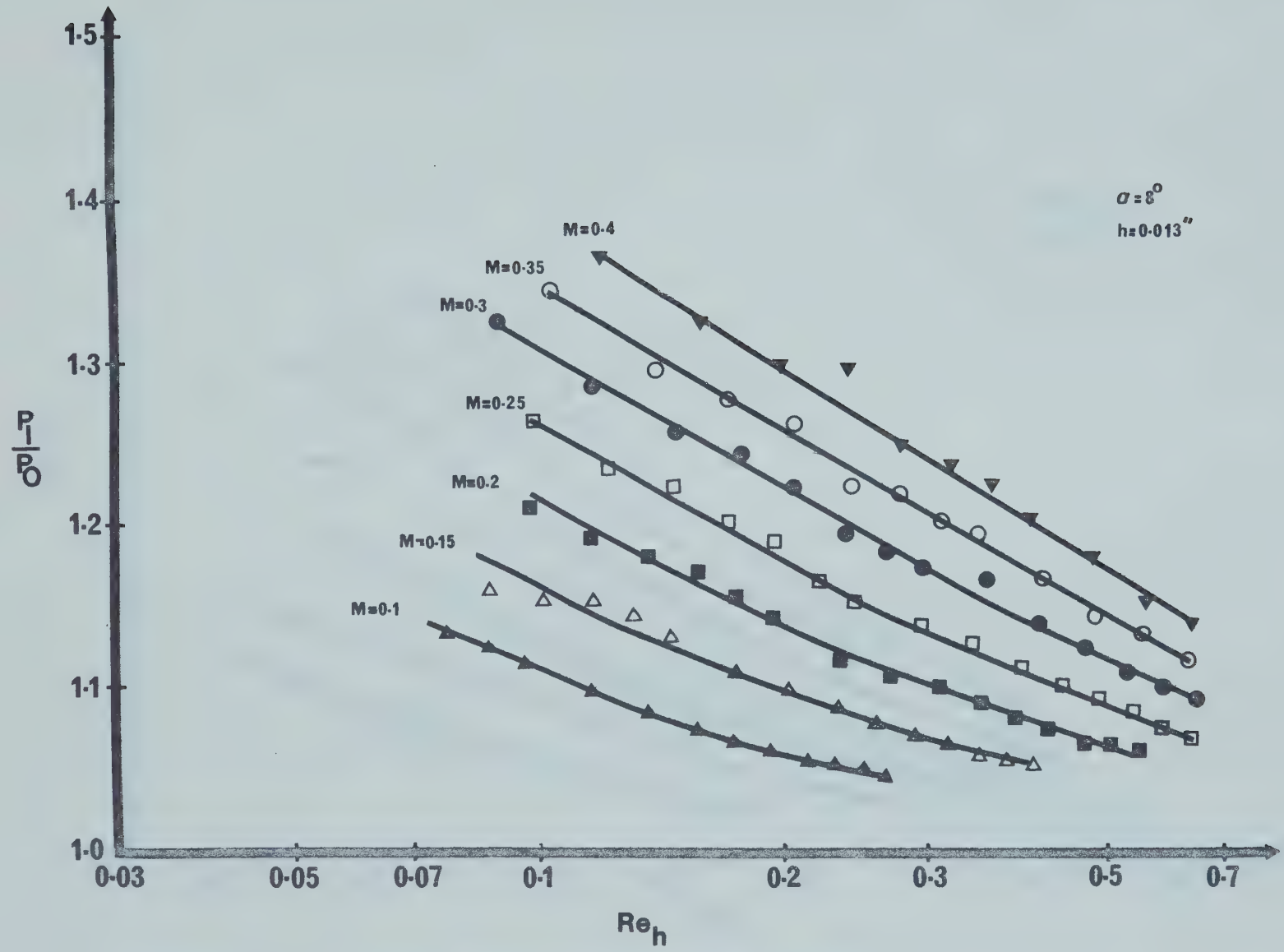

FIGURE 14. Wedge Probe Correction Factors;
8° Wedge, h=0·013 inches

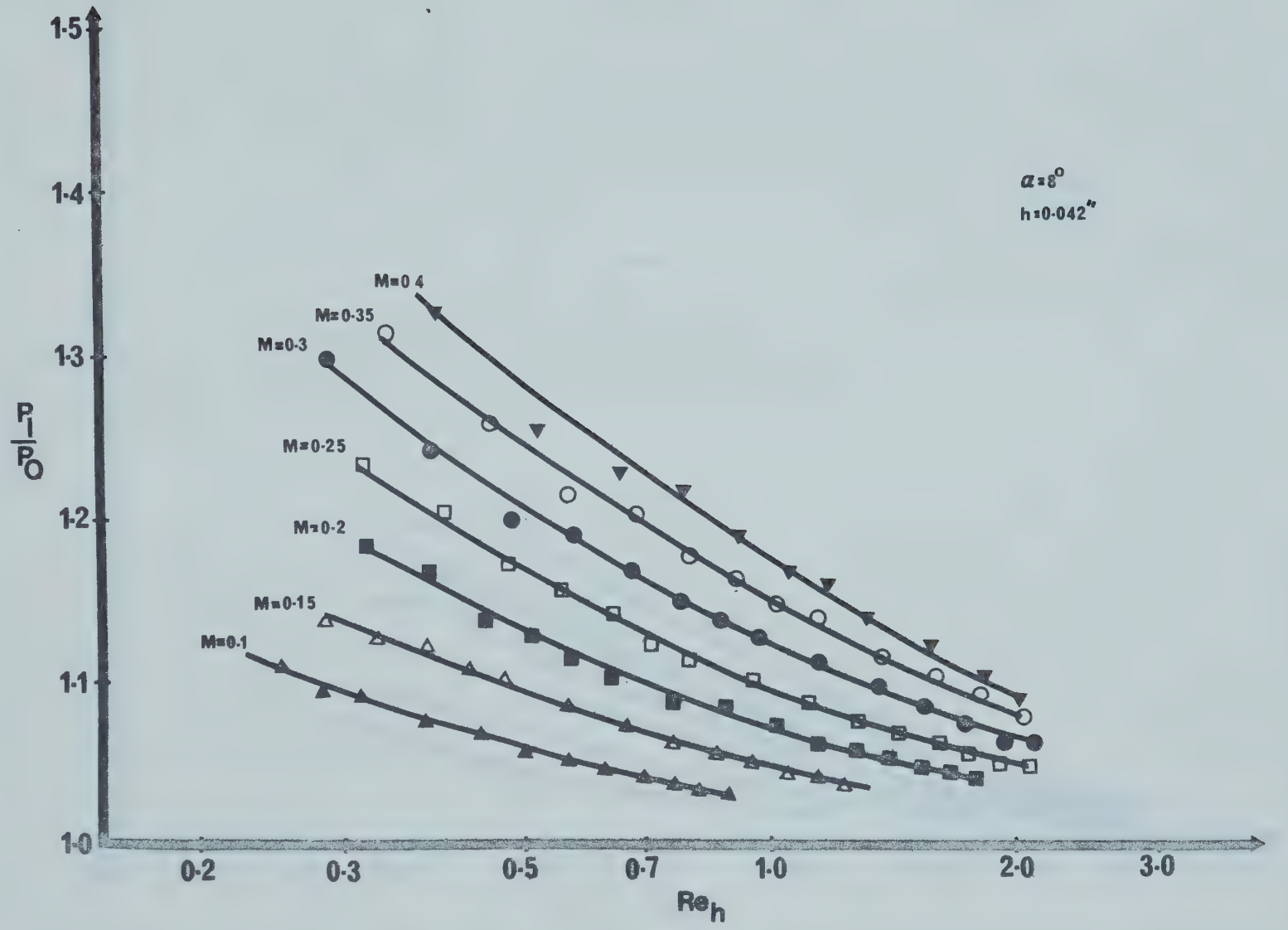

FIGURE 15. Wedge Probe Correction Factors;
8° Wedge, h=0·042 inches

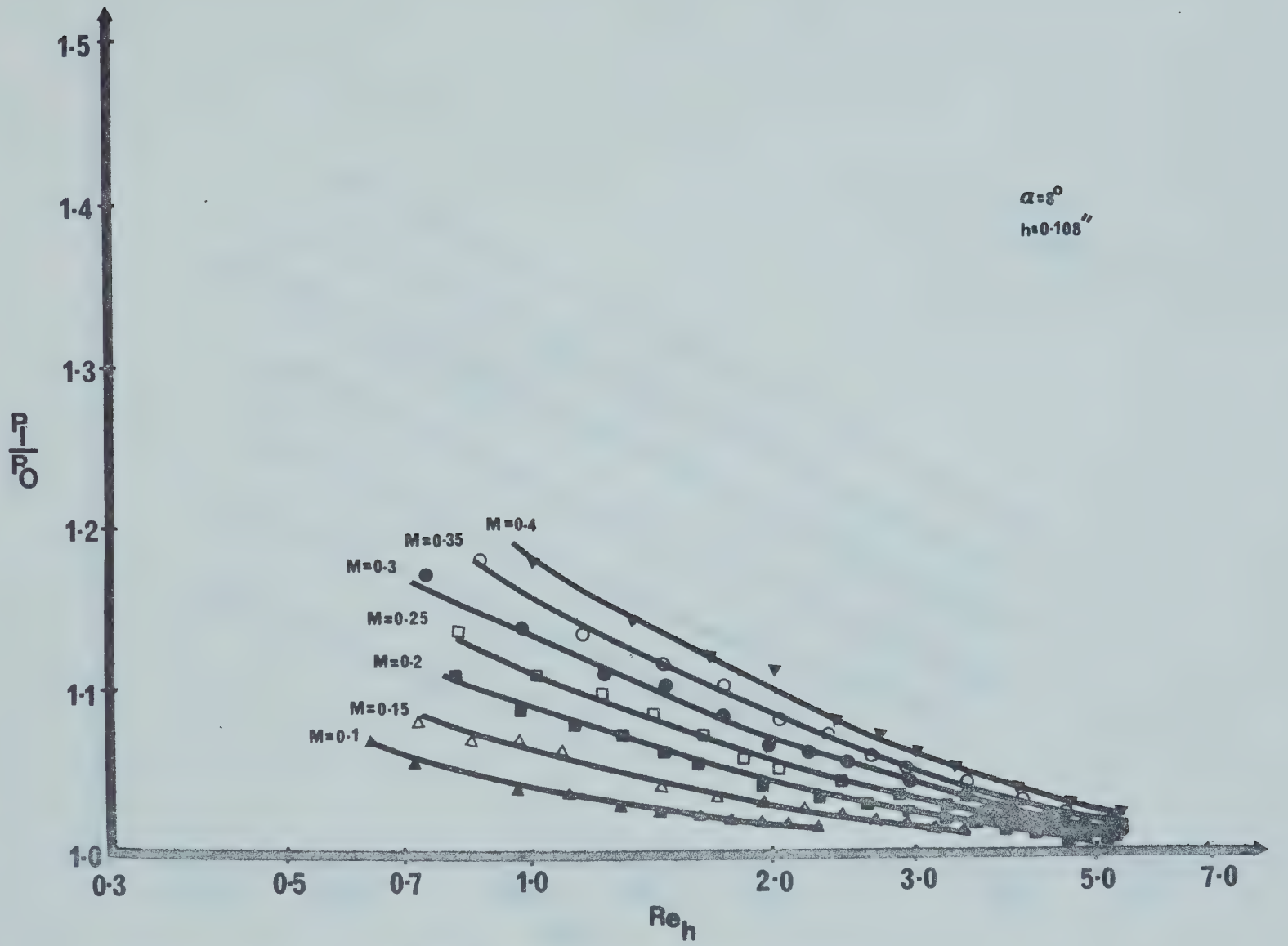

FIGURE 16. Wedge Probe Correction Factors;
8° Wedge, h=0·108 inches

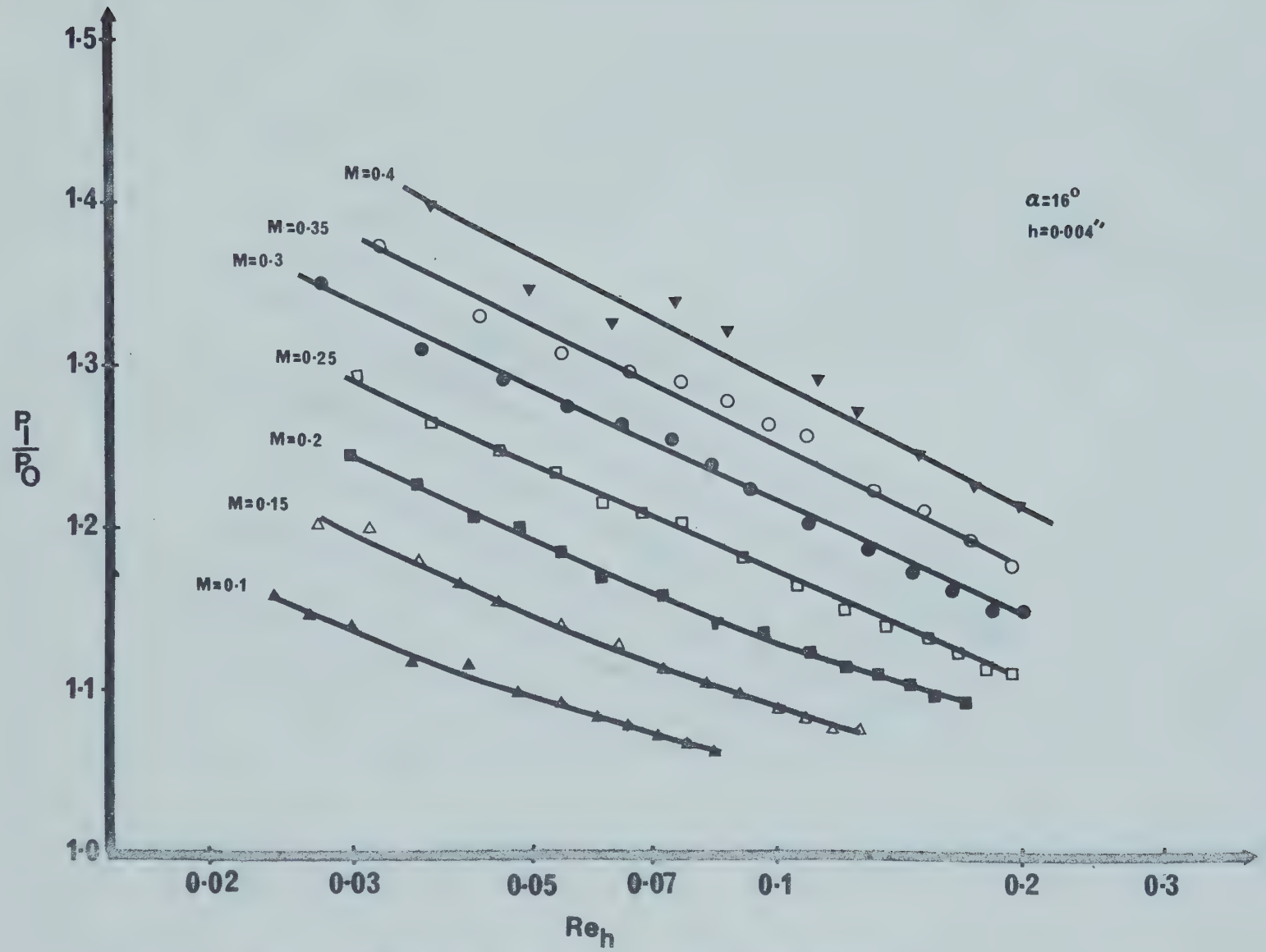

FIGURE 17. Wedge Probe Correction Factors; 16° Wedge, h=0·004 inches

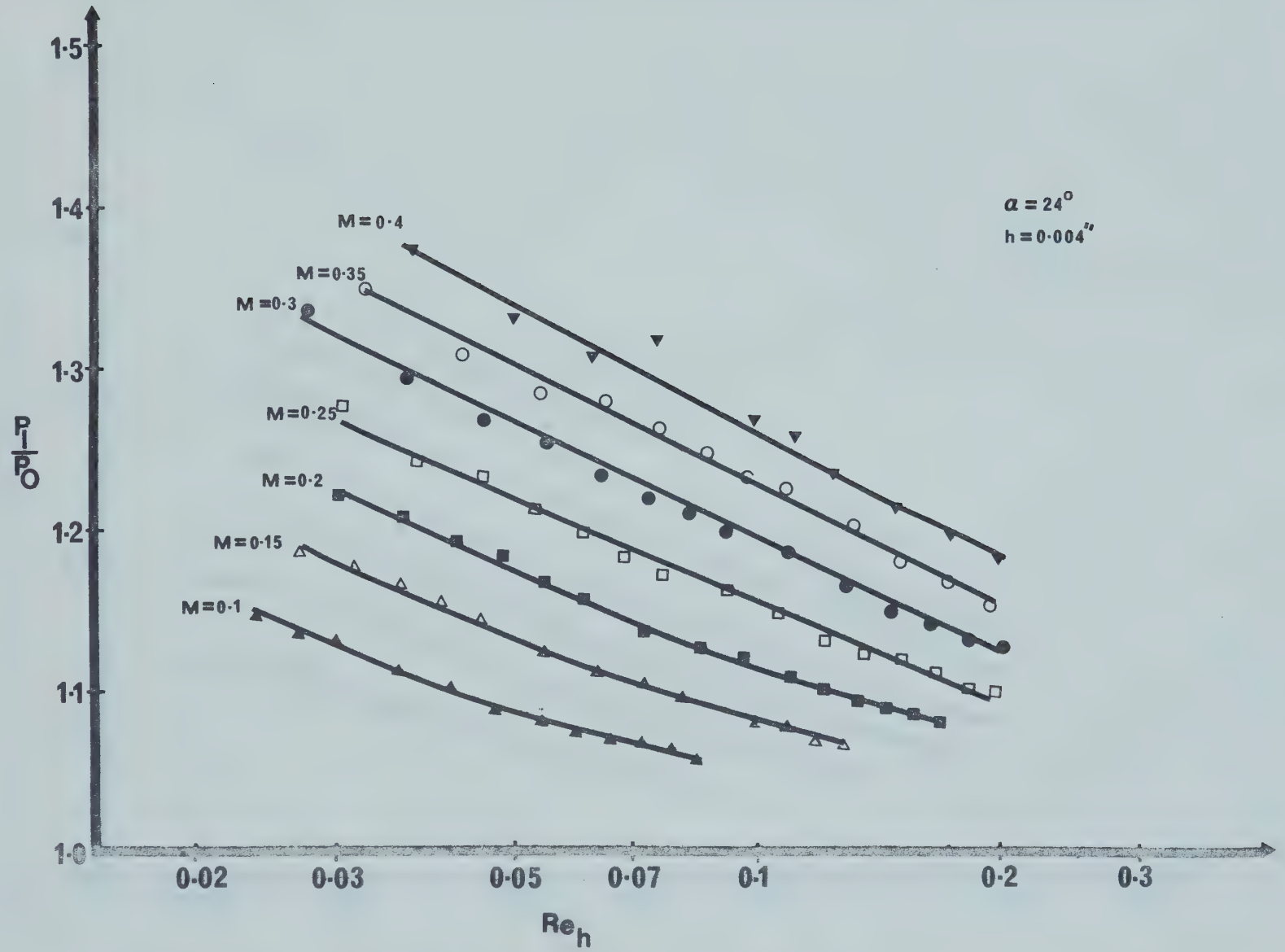

FIGURE 18. Wedge Probe Correction Factors;
8° Wedge, h=0·004 inches

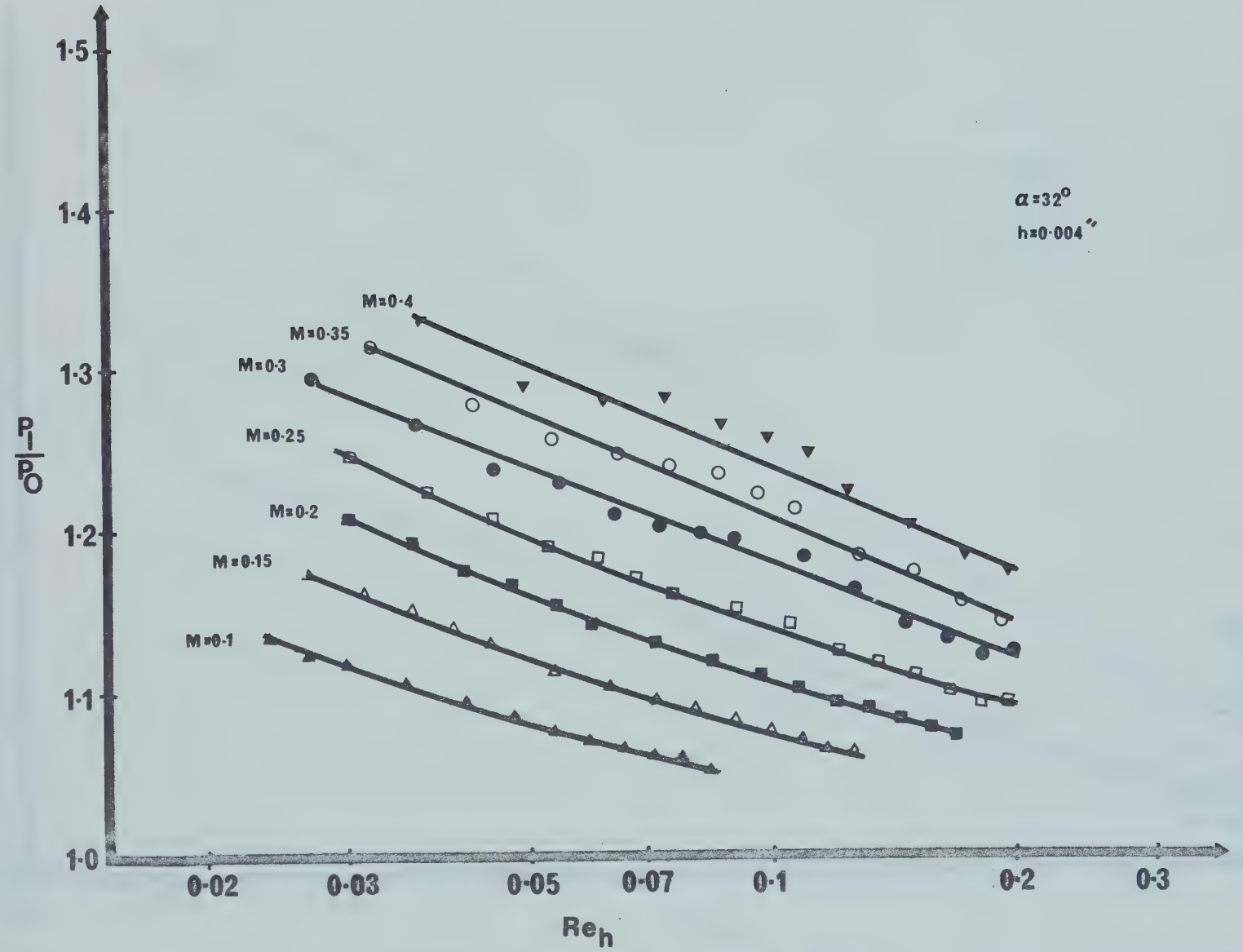

FIGURE 19. Wedge Probe Correction Factors; 32° Wedge, h=0·004 inches

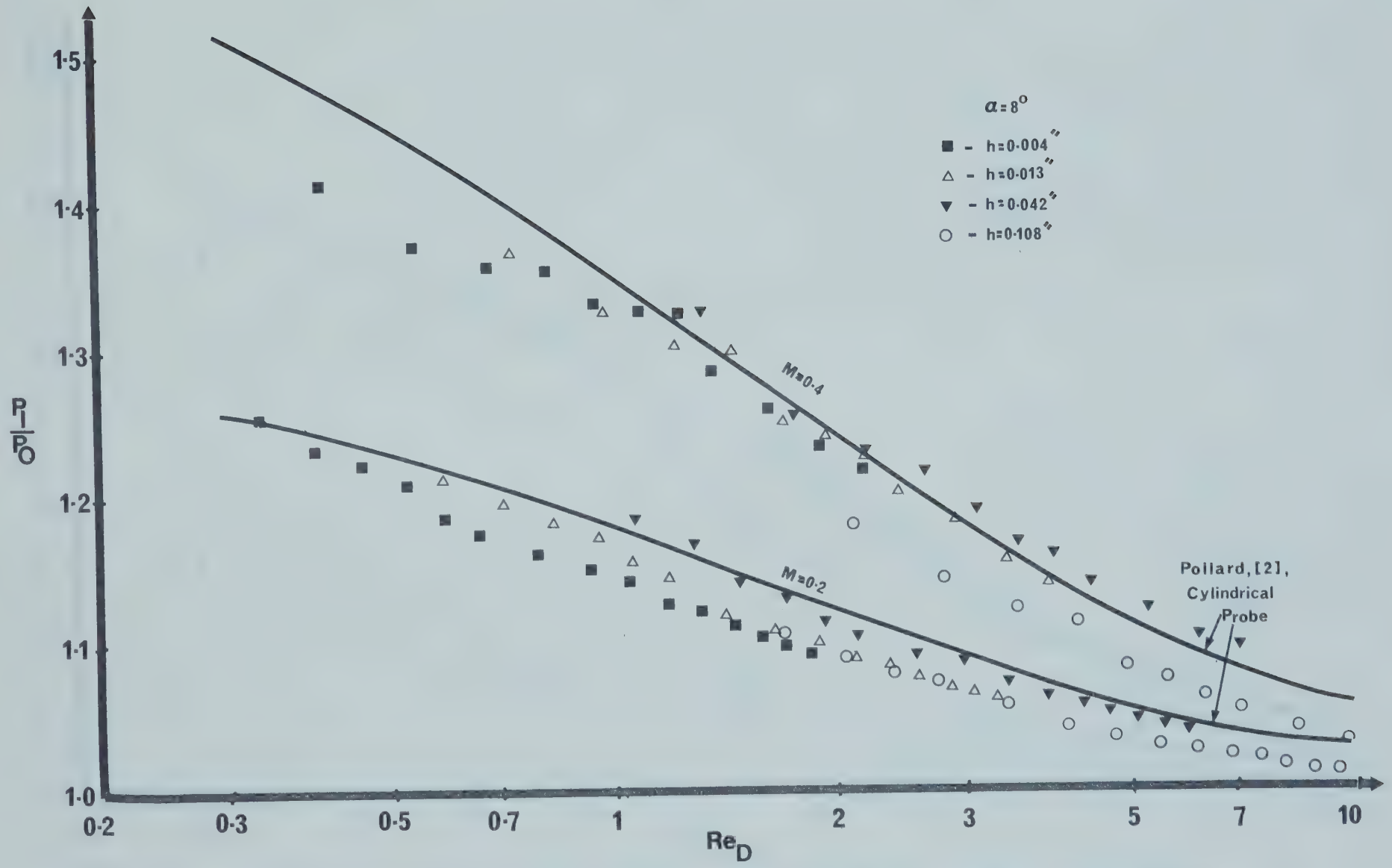

FIGURE 20. Correction Factors for 8° Wedge Probes as a Function of Reynolds Number based on Equivalent Diameter, M=0·2 , 0·4

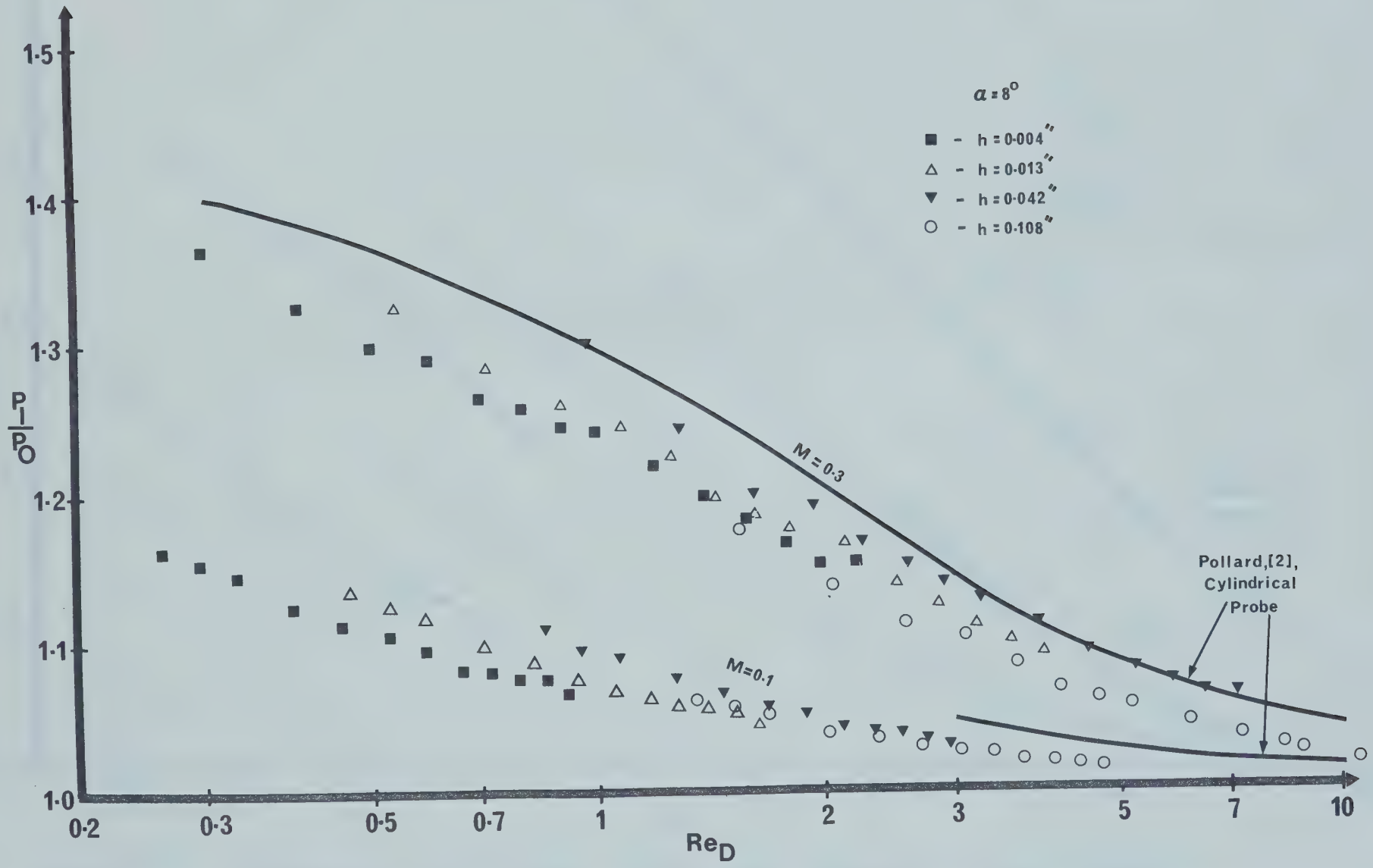

FIGURE 21. Correction Factors for 8° Wedge Probes as a Function of Reynolds Number based on Equivalent Diameter, M = 0·1, 0·3

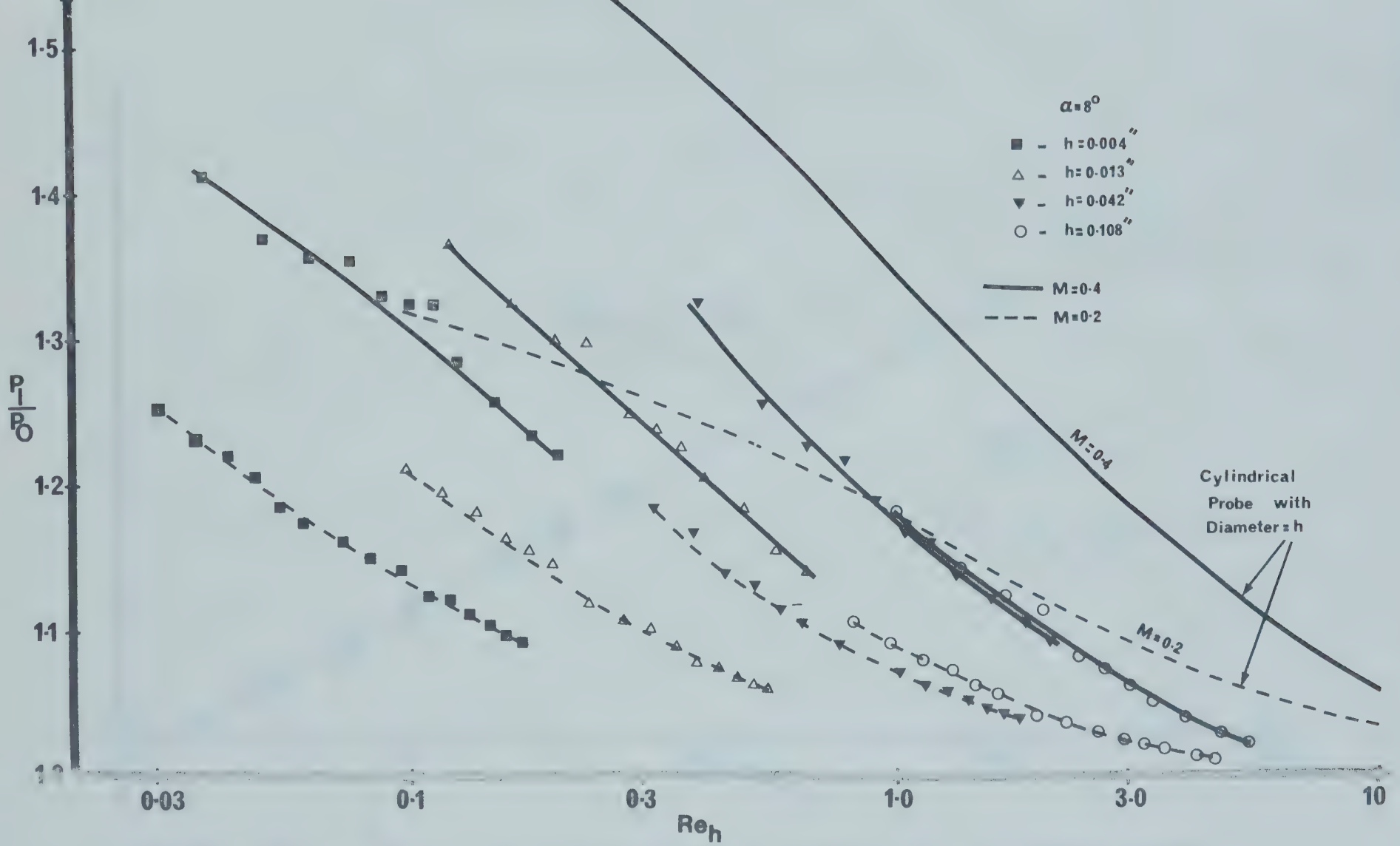

FIGURE 22. Comparison of 8^0 Wedge Probes with Cylindrical Probes, Reynolds Numbers based on Orifice height, M = 0·2, 0·4

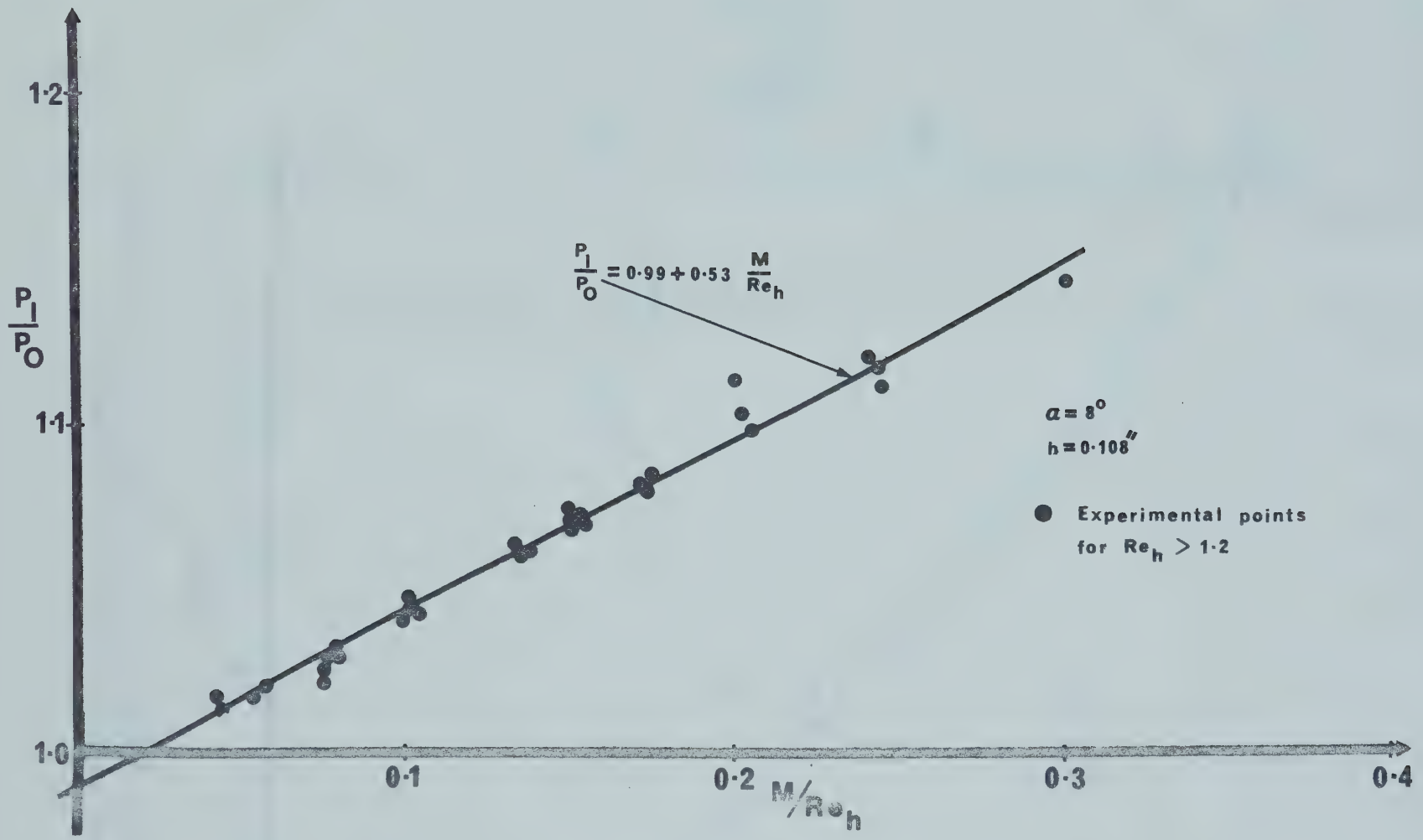

FIGURE 23. M/Re_h as a Correlating Parameter for 8° Wedge Probe with Orifice Height 0·108 inches

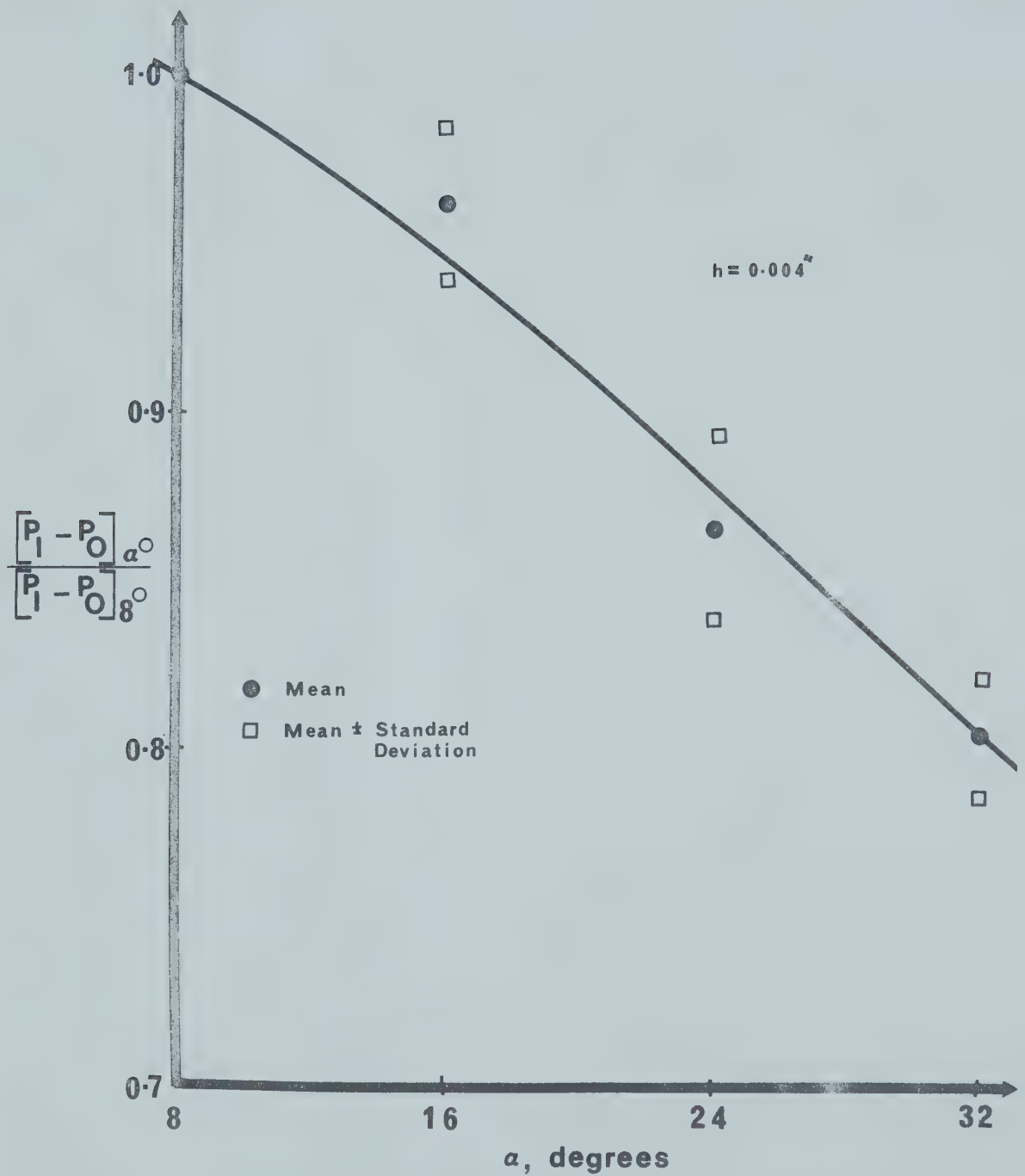

FIGURE 24. Viscous Correction Ratios as a Function of Probe Wedge Angle